Journal of Geosciences, 69 (2024), 231–249 DOI: 10.3190/jgeosci.400

Original paper

Mineralogy of metamorphic magnetite-manganese ores at the Prakovce–Zimná Voda prospect (Spišsko-gemerské rudohorie Mts., Slovakia): The occurrence of REE-bearing allanite-subgroup minerals ferriakasakaite and ferriallanite

Pavol MYŠĽAN[1,2]*, Martin ŠTEVKO[1,3], Tomáš MIKUŠ[4]

[1] *Earth Science Institute, Slovak Academy of Sciences, Dúbravská cesta 9, P. O. BOX 106, 840 05 Bratislava, Slovakia; pavol.myslan@savba.sk*

[2] *Department of Mineralogy, Petrology and Economic Geology, Faculty of Natural Sciences, Comenius University in Bratislava, Ilkovičova 6, Mlynská dolina, 842 15 Bratislava, Slovakia*

[3] *Department of Mineralogy and Petrology, National Museum, Cirkusová 1740, 193 00 Praha 9-Horní Počernice, Czech Republic*

[4] *Earth Science Institute, Slovak Academy of Sciences, Ďumbierska 1, 974 11 Banská Bystrica, Slovakia*

* *Corresponding author*

Manganese mineralization was discovered at the Zimná Voda occurrence near Prakovce located in the Spišsko-gemerské rudohorie Mountains, eastern Slovakia. The mineralization is hosted in the Early Paleozoic metamorphic rocks of the Gemeric Unit in the Western Carpathians and it represents the only occurrence of metamorphosed manganese mineralization discovered within the Drnava Formation (Devonian). Manganese minerals are directly associated with magnetite bodies forming isolated lenses of a strata-bound oxidic Fe-ores. The manganese mineralization underwent metamorphism during the Variscan and Alpine tectonometamorphic events, resulting in two types of distinct mineral assemblages. The older assemblage includes rhodonite–ferrorhodonite series, rhodochrosite, kutnohorite, spessartine, fluorapatite and quartz with magnetite impregnations. These assemblages are intersected by younger mineral assemblages present in veins and vugs. This later assemblage consists of rhodochrosite, kutnohorite, baryte, clino-suenoite to clino-ferro-suenoite, minerals of the epidote supergroup, quartz and relatively rare sulfidic mineralization including pyrite, galena, sphalerite and cobaltite along with hübnerite. This stage also features the formation of garnets predominantly composed of the andradite molecule, with locally preserved spessartine remnants in the garnet centres. The subsequent younger post-Variscan metamorphic event is characterized by a high influx of rare earth elements (REE), leading to the formation of a rare ferriallanite-(Ce), ferriallanite-(La), ferriakasakaite-(La) and ferriakasakaite-(Ce). Allanite-subgroup minerals form a strongly zonal polycrystalline dark brown aggregates with size up to 50 μm, generated from hydrothermal fluids affecting the mineral composition of the late-stage mineral assemblage.

Keywords: magnetite, rhodonite, spessartine, andradite, epidote supergroup, ferriakasakaite series, Spišsko-gemerské rudohorie Mts.
Received: 10 July 2024; accepted: 30 December 2024; handling editor: F. Laufek
The online version of this article (doi: 10.3190/jgeosci.400) contains electronic supplementary material.

1. Introduction

Manganese deposits with abundant iron content represent an interesting type of mineralization, generated by numerous sedimentary, magmatic, hydrothermal, biogenic or metasomatic (skarn) processes, such as element precipitation from hydrothermal fluids and sediments pore water, metasomatic replacements, hydrogenetic precipitation or microbial activity, resulting in formation of volcanogenic, magmatic-hydrothermal, sedimentary exhalative, skarn-like or many more deposits (Roy 1992; Hein et al. 1997, etc.).

The metamorphosed manganese mineralization in the Western Carpathian region with variable mineral assemblage is recently studied at the different localities situated in the Spišsko-Gemerské Rudohorie Mountains., mostly located in the Southern Gemeric Unit (Čučma–Čierna baňa, Malá Hekerová–Bystrý potok near Smolník, Betliar–Július). The Mn mineralization is represented by silicate-carbonate lenses with manganese minerals, situated in the metavolcano–sedimentary rocks metamorphosed within the greenschist facies conditions of the Gelnica Group. Various mineral phases (approximately 100 identified minerals) and genetic data (e.g. rhodonite-pyroxmangite geothermometer) provide evidence of polygenetic origin (Kantor 1953a, b; Faryad 1994; Peterec and Ďuďa 2003; Rojkovič 2001; Števko et al. 2015; Radvanec and Gonda, 2020; Myšľan et al. 2023, etc.), with the first description of ferriandrosite-(Ce) at the locality Betliar–Július (Števko et al. 2023). In the Northern Gemeric Unit, more specifically in the Rakovec Group,

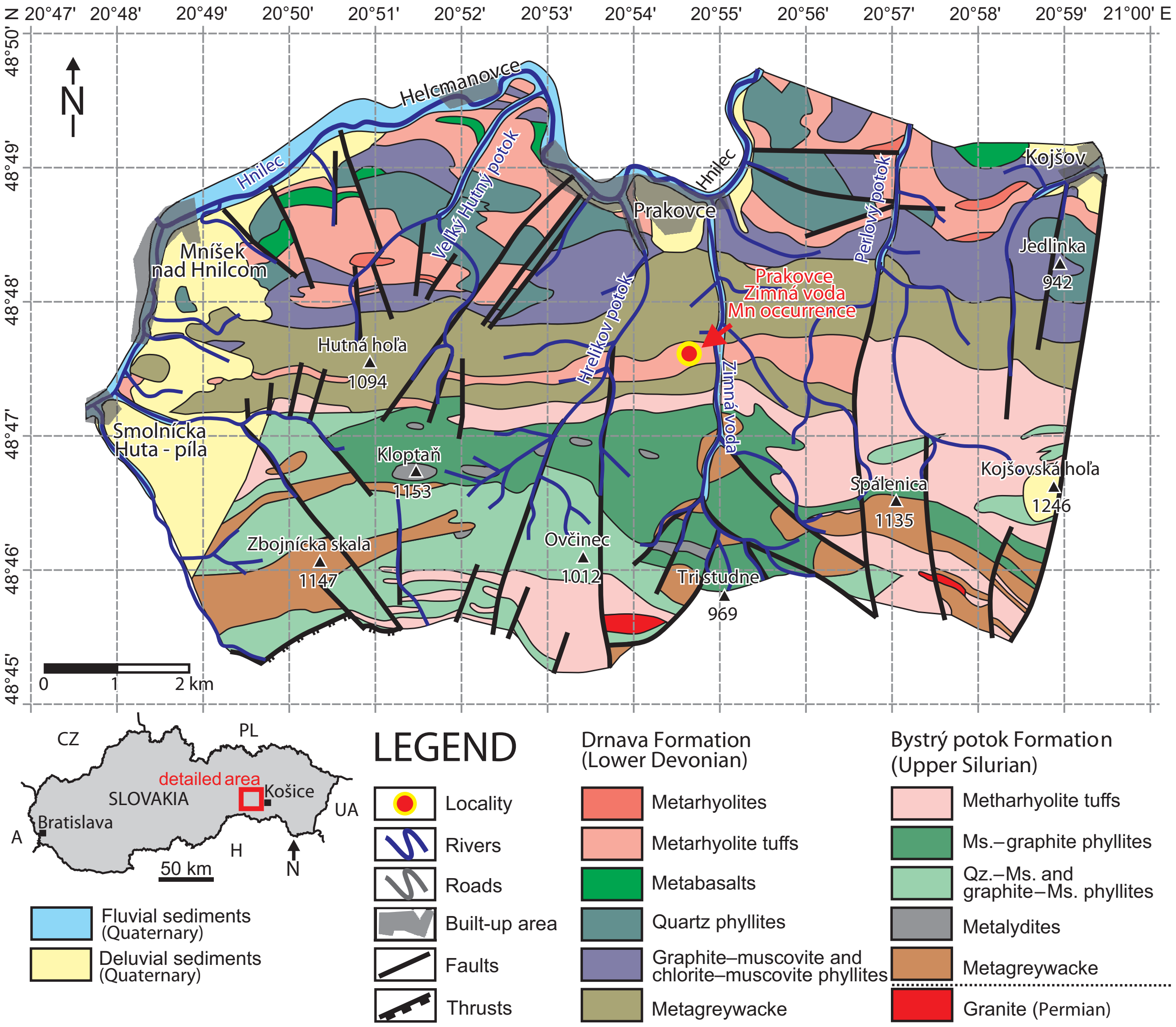

Fig. 1 Geological map of the studied area with marked location of Prakovce–Zimná Voda manganese occurrence (modified after Bajaník et al. 1983).

a 22 m thick layer of manganese enriched metasediments was described from the RHV-1 borehole situated south of Rudňany, where piemontite and spessartine aggregates alongside with Fe oxides were present in the form of Mn–Fe nodules (Spišiak et al. 1989; Spišiak and Hovorka 2000). New occurrence of As-enriched manganese mineralization was discovered at the Poráč–Diely occurrence with unique mineral assemblage consisting of, among other silicates and carbonates, Li-pyroxenoids, arsenosilicates and arsenates (Myšľan et al. 2024).

Mineralogy of the Prakovce–Zimná Voda manganese occurrence has never been studied in detail. The presence of manganese mineralization in this region was briefly described by Zipser (1817) and later by Leonhard (1843) who mentioned that it is consisting of orange to red leaf-like aggregates of rhodonite and rhodochrosite in association with magnetite. More recent studies reported tens of meters long and 0.5–3 m thick lenses with hematite-magnetite mineralization, in which rhodochrosite is locally bound in the area east of Zimná dolina valley (Grecula et al. 1995). This locality is representing the only known occurrence of metamorphic manganese ores in the Drnava Formation.

Our study provides a considerable amount of a detailed crystallochemical data of the minerals at the studied locality, focusing on the characterization of minerals of the allanite-subgroup, as well as comparison of these data with the analogous occurrences in the Carpathian area and the other relevant localities in the world.

2. Geological settings and location

Manganese mineralization at the Prakovce–Zimná Voda occurrence is hosted in the Early Paleozoic low-grade metamorphic rocks of the Gemeric Unit in the northeastern part of the Spišsko-Gemerské Rudohorie Mts., Eastern Slovakia. The Gemeric Unit is composed of Lower Paleozoic basement (Gelnica and Rakovec Group), Upper Paleozoic (Ochtiná, Dobšiná and Gočaltovo Group) and Lower Triassic (Kobeliarovo Group) cover complexes (Bajaník et al. 1983). The Lower Paleozoic Gemeric basement units are considered to be riftogenic basin origin associated with Gondwana active margin (Grecula 1982; Putiš et al. 2008). Complexes were intruded by the Permian S-type Gemeric granites (Uher and Broska 1996).

The Gelnica Group is metamorphosed formation with characteristic polygenetic and polycyclic development defined by cyclic marine pelite–psammite flyschoid sedimentation and syngenetic silicic (dacite to rhyolite) and, to a lesser extent, basic volcanism. Metasedimentary complexes dominantly consist of metamorphosed sandstones, pelites and psamites with significant incorporation of volcano-clastic material. The Gelnica Group is divided into Vlachovo, Bystrý Potok and Drnava Formations (Bajaník et al. 1983). Drnava Formation in the northern part of Gelnica Group (Fig. 1) is in the basal parts formed by metamorphosed coarse-grained sandstones with rapid transition to fine-grained conglomerates in the upper parts. Concurrent volcanic activity is characterised by presence of acidic volcano-clastic material transported into the sedimentary basin alongside with epiclastic detritus. Effusive forms of volcanism have been detected only sporadically with volcanic cycles terminated by basic volcanic members identified in the form of their redeposited volcanoclastic equivalents (Bajaník et al. 1983). The age of the Drnava Formation was determined biostratigraphically to Lower Devonian (Snopková and Snopko 1979), the U–Pb SHRIMP dating of zircons from metarhyolite pyroclastic rocks show age around 460 Ma, corresponding to the Middle Ordovician (Darriwilian) age (Vozárová et al. 2017). Metamorphic conditions determined from the Early Paleozoic metasedimentary and metavolcanic rocks of the Gelnica Group range from 300 to 440 °C at 300–700 MPa (Sassi and Vozárová 1987; Mazzoli and Vozárová 1989). These conditions correspond with geothermometric calculations from metamorphic manganese ores at the similar Mn occurrence near Čučma, with estimated P–T parameters at 375 ± 10 °C (Faryad 1991), 390 °C (Rojkovič 1999), and 400–420 °C at 320–370 MPa with $X\mathrm{CO_2} = 0.055–0.060$ (Faryad 1994). Lenses with metamorphic magnetite–manganese ore mineralization near Prakovce are hosted in the narrow strip of metavolcano-clastic rocks represented by metarhyolite tuffs of the Drnava Formation, whereas other localities in Southern Gemeric Unit are hosted in rocks belonging to the Bystrý Potok Formation.

Hematite–magnetite ore mineralization developed in the Early Paleozoic volcanogenic–sedimentary formations of the Gemeric Unit is related to bimodal volcanic activity resulting in formation of strata-bound oxidic Fe-ores. Ore mineralization appears in the various forms, mostly as magnetite and hematite impregnations, to a lesser extent as hematite quartzites or jaspilites in association with surrounding volcano–sedimentary rocks. Magnetite impregnations may be clustered into the larger accumulations forming magnetite lenses and bodies. These ores mostly occur in the lower parts of the uppermost formations, frequently represented by metarhyolite tuffs (Grecula et al. 1977, 1995).

The Prakovce–Zimná Voda manganese occurrence is situated approximately 2.5 km SSE of the Prakovce village (Gelnica district, Košice region) on the western slopes of the Gelnická valley. The locality consists of multiple small exploration pits, open-pit works and collapsed adit. Samples with manganese ore were collected at the small pit with GPS coordinates 48°47'41.7"N and 20°54'33.0"E (at altitude 578 m a.s.l.) and at the ore dump from the open-pit work with GPS coordinates 48°47'42.7"N and 20°54'37.6"E (at altitude 554 m a.s.l.).

3. Analytical methods

The representative samples of metamorphosed manganese mineralization were collected in the 2023, from which series of polished thin sections and mounts were prepared from the upper small pit (PRH-1 to PRH-6) and from the lower dump (PRD-1 to PRD-12).

Quantitative chemical (WDS) analyses of studied minerals were obtained using a JEOL-JXA850F field-emission electron microprobe (EMPA) in wavelength-dispersive spectrometry (WDS) mode (Earth Science Institute, Slovak Academy of Sciences, Banská Bystrica, Slovakia). The following conditions were applied: accelerating voltage 15 kV, measuring current 20 nA (silicates, carbonates and sulfates) and accelerating voltage 20 kV and measuring current 15 nA (sulfides). The beam diameter ranged from 1 to 8 µm, ZAF correction was used. The following standards and X-ray lines were used: albite (Al*Kα*, Na*Kα*), Ag (Ag*Lα*), baryte (S*Kα,* Ba*Lα*), CdTe (Cd*Lα*), celestine (Sr*Lα*), $\mathrm{CePO_4}$ (Ce*Lα*), crocoite (Pb*Mβ*), $\mathrm{Cr_2O_3}$ (Cr*Kα*), Co (Co*Kα*), $\mathrm{CuFeS_2}$ (Cu*Kα*), diopside (Si*Kα*, Mg*Kα*, Ca*Kα*), $\mathrm{DyPO_4}$ (Dy*Lβ*), $\mathrm{ErPO_4}$ (Er*Lα*), $\mathrm{EuPO_4}$ (Eu*Lα*), fluorapatite (P*Kα*), fluorite (F*Kα*), GaAs (As*Lα*), gahnite (Zn*Kα*), $\mathrm{GdPO_4}$ (Gd*Lβ*), Ge (Ge*Lα*), hematite (Fe*Kα*), HgTe (Hg*Lα*), $\mathrm{HoPO_4}$ (Ho*Lβ*), InAs (In*Lα*), $\mathrm{LaPO_4}$ (La*Lα*), $\mathrm{LuPO_4}$ (Lu*Lα*), $\mathrm{Ni_2Si}$ (Ni*Kα*), $\mathrm{NdPO_4}$ (Nd*Lα*), orthoclase (K*Kα*), PbSe (Se*Lβ*), PbTe (Te*Lα*), $\mathrm{PrPO_4}$ (Pr*Lβ*), rhodonite (Mn*Kα*), rutile (Ti*Kα*), $\mathrm{Sb_2S_3}$ (Sb*Lα*), $\mathrm{ScVO_4}$ (V*Kα*), $\mathrm{SmPO_4}$ (Sm*Lβ*), $\mathrm{ThO_2}$ (Th*Mα*), $\mathrm{TbPO_4}$ (Tb*Lα*), $\mathrm{TmPO_4}$ (Tm*Lα*), $\mathrm{UO_2}$ (U*Mβ*), tugtupite (Cl*Kα*), $\mathrm{YbPO_4}$ (Yb*Lα*), and $\mathrm{YPO_4}$ (Y*Lα*). The

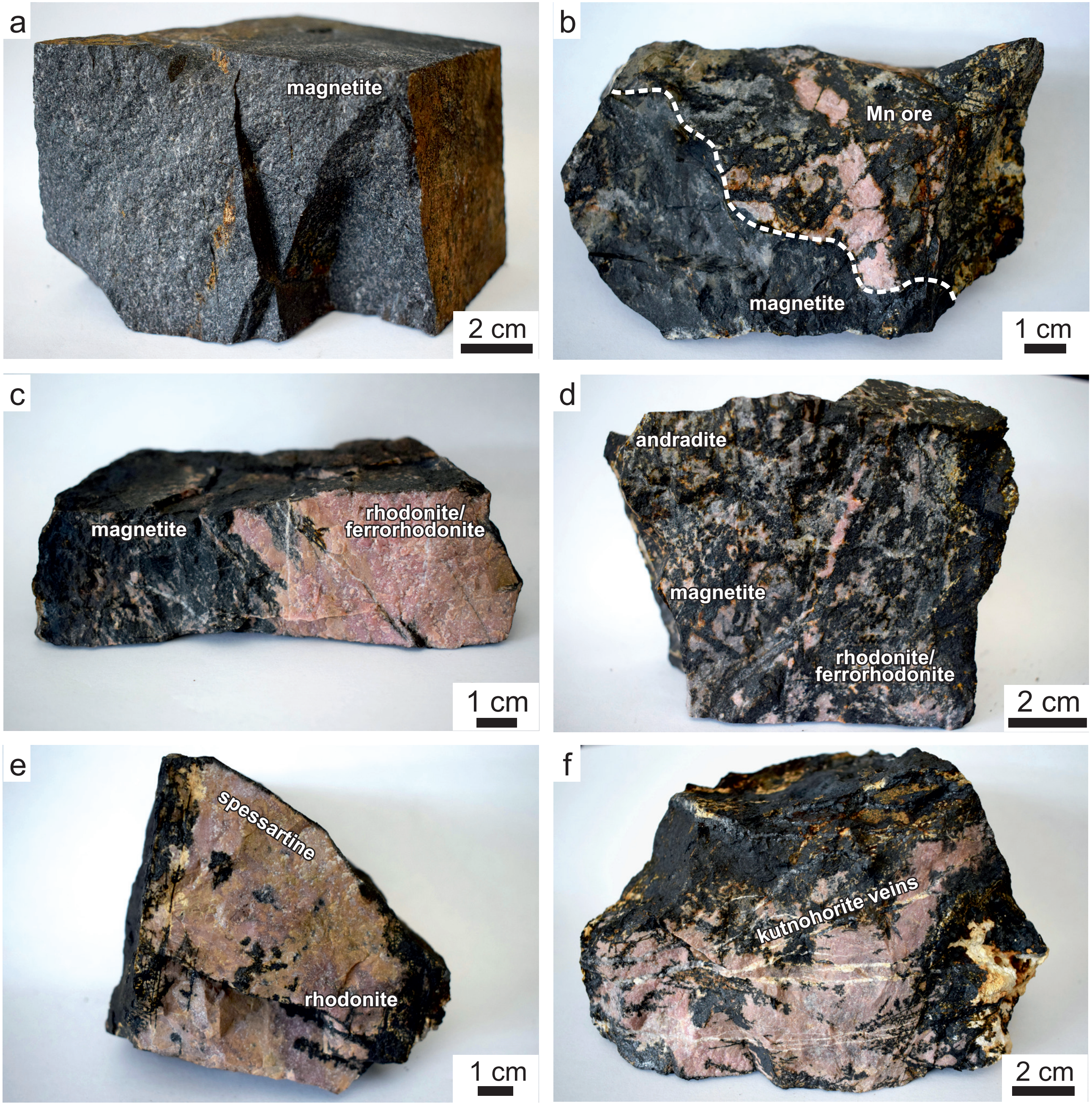

Fig. 2 Textural photographs of a representative studied samples of magnetite lenses and manganese mineralization from the locality Prakovce–Zimná Voda. **a** – Massive magnetite from the associating magnetite lenses. **b** – Contact zone (highlighted by dotted line) of magnetite body and manganese ore, consisting of pink rhodonite–ferrorhodonite series, magnetite (black), andradite (green) and other Mn-rich minerals. **c** – Mixed mineral association composed of minerals from magnetite lenses and manganese mineralization. **d** – Sharp contact of magnetite lense with Mn-rich matrix composed of rhodonite-ferrorhodonite series. **e** – Manganese ore composed of pink rhodonite and yellow spessartine. **f** – Advanced oxidization of manganese ore cut by a system of a whitish kutnohorite veins.

⇨

Fig 3 BSE images of minerals forming the dominant components of manganese ore at the locality Prakovce–Zimná Voda. **a** – Fine-grained magnetite lens at the contact with manganese ore consisting of rhodonite cut by younger kutnohorite–amphibole vein. **b** – Rhodochrosite vein cutting rhodonite matrix with kutnohorite-spessartine accumulations in rhodonite matrix. **c** – Porous andradite in rhodonite matrix pushing magnetite impregnations. **d** – Spessartine relicts outgrown by andradite crystals grouped to an external rim, **e** – Porous andradite in association with magnetite anhedral grains in rhodonite matrix. **f** – Clino-suenoite and clino-ferro-suenoite in the interstitial places between rhodonite crystals and quartz. **g** – Fluorapatite grains in rhodochrosite, **h** – Baryte grains in rhodonite cavities filled with rhodochrosite and clino-suenoite.

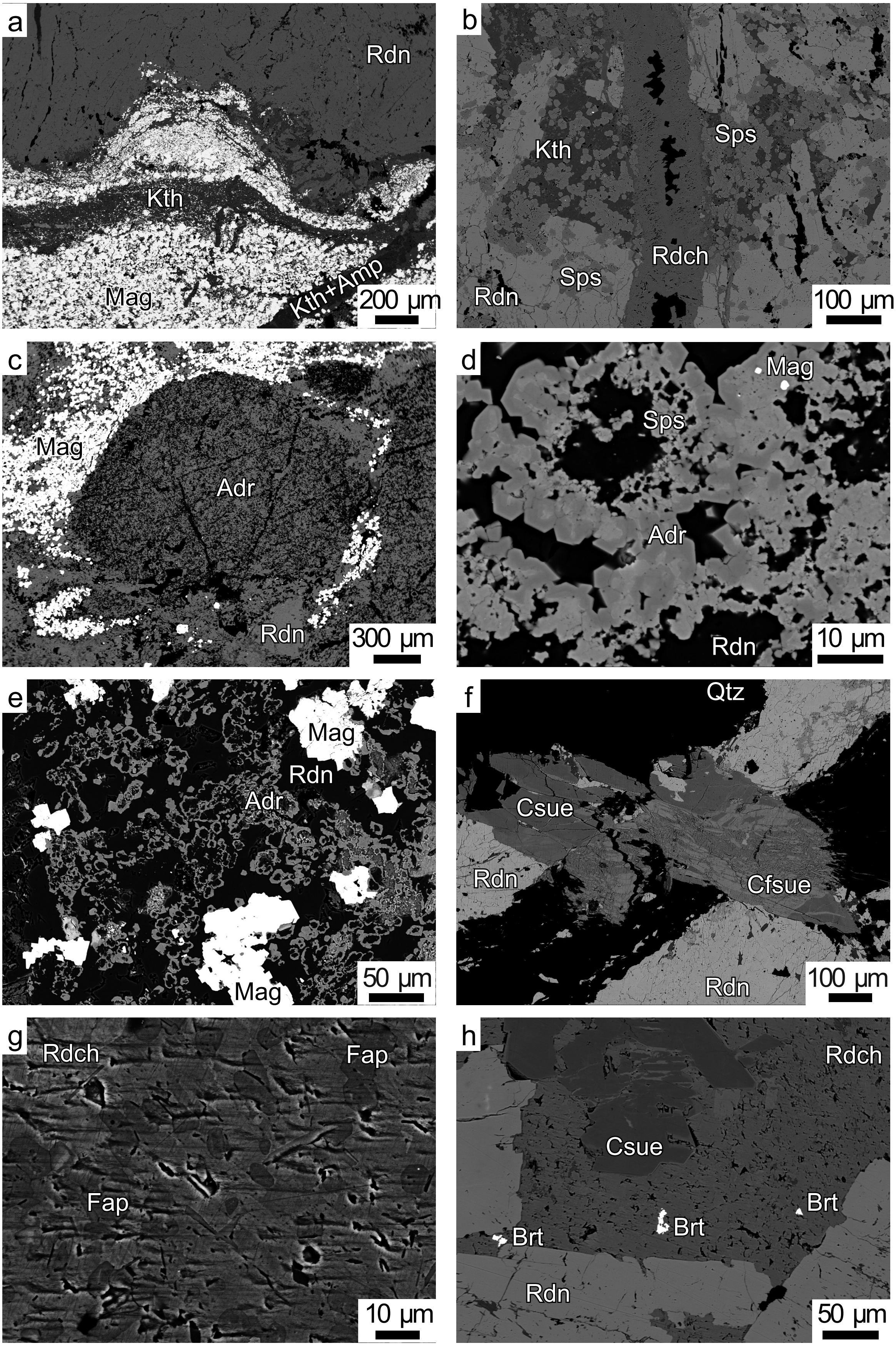
a
Rdn
Kth
Mag
Kth+Amp
200 µm
b
Kth
Sps
Rdch
Sps
Rdn
100 µm
c
Mag
Adr
Rdn
300 µm
d
Mag
Sps
Adr
Rdn
10 µm
e
Mag
Rdn
Adr
Mag
50 µm
f
Qtz
Csue
Rdn
Cfsue
Rdn
100 µm
g
Rdch
Fap
Fap
10 µm
h
Rdch
Csue
Brt
Brt
Brt
Rdn
50 µm

detection limit of every element ranged from 0.002–0.030 wt. %. Elements which were analysed quantitatively and are below the detection limit are not listed in the tables. The procedures for calculating the individual empirical formulae of the studied minerals were according to the currently valid nomenclatures by Armbruster et al. (2006) for the epidote-group minerals, Grew et al. (2013) for the garnet supergroup, Hawthorne et al. (2012) for amphibole supergroup minerals, Bosi et al. (2019) for spinel supergroup and Shchipalkina et al. (2019) for rhodonite-group minerals. Procedures are listed together with all chemical analyses in Electronic Supplementary Material (ESM1). Photographic documentation of relationships between minerals was carried out in the BSE mode. Abbreviations of minerals are defined in Warr (2021).

Powder X-ray diffraction (PXRD) data for rhodonite were obtained on a Bruker D8 Advance diffractometer equipped with solid-state LynxEye detector and secondary monochromator producing Cu$K\alpha$ radiation at the Department of Mineralogy and Petrology, National Museum in Prague. The analyses were conducted at 40 kV and 40 mA. The powder samples were placed on the surface of a flat Si plate infused in acetone suspension. The powder pattern was collected in the Bragg-Brentano geometry with step 0.01° 2θ with counting time of 8 s per step.

4. Results

4.1. Textural features of magnetite–manganese mineralization

The manganese mineralization is embedded in the several meters thick magnetite bodies, forming massive lenses of irregular shapes embedded in metarhyolite tuffs and tuffites. Magnetite accumulations form massive black aggregates with metallic lustre, associated with quartz (Fig. 2a). Close to the contact with acid metavolcanic rocks, mineralization is often arranged in strips and laminae. In the magnetite lenses, the accumulations of manganese minerals occur, forming up to 30 cm thick blocks.

Close to the contact with magnetite bodies, rhodochrosite and kutnohorite occurs in interstitial spaces within the individual magnetite crystals. The boundary between the magnetite bodies and the manganese mineralization composed mostly by rhodonite–ferrorhodonite series in matrix is well-defined (Fig. 2b, c). This sharp contact is marked by a thin and irregular zone, ~30 µm wide, consisting of Mn-carbonates (Fig. 3a). To a certain extent, near the contact zone an intimate overgrowth of magnetite and manganese ore can be observed, forming pink, yellow, green and black masses (Fig. 2d).

Manganese mineralization is macroscopically dominantly light to dark pink and yellow colour (Fig. 2e) cut by the younger system of white coloured veins with a thickness up to 0.3 cm (Fig. 2f). Mineralization is dominantly formed by rhodonite–ferrorhodonite series, rhodochrosite, kutnohorite, quartz, spessartine, andradite, minerals of amphibole supergroup and magnetite with locally enriched accumulations of fluorapatite. Accessory minerals include minerals of epidote supergroup, baryte, galena, sphalerite, pyrite, cobaltite, and rare hübnerite. The massive manganese ore is cut by quartz, kutnohorite, rhodochrosite and amphibole veins. Secondary manganese oxides and hydroxides were also observed forming dark brown to black peripheral zones within the manganese ore (Fig. 2c-f).

4.2. Mineral association in magnetite–manganese ore

4.2.1. Magnetite

Magnetite–manganese ore is dominantly composed of subhedral to anhedral crystals of magnetite with average size approximately 30 µm in diameter (Fig. 3a). Magnetite from magnetite lenses that do not contain manganese mineralization show a homogenous chemical composition close to ideal end-member formula with slightly elevated content of MnO (up to 0.4 wt. %; 0.01 *apfu* Mn) (Tab. 1, ESM1). Magnetite associated with manganese minerals forms isolated crystals and aggregates which shows similar chemical composition close to the ideal end-member formula with slightly elevated content of MnO (up to 0.2 wt. %; 0.01 *apfu* Mn) (Tab. 1, ESM1).

4.2.2. Rhodonite–ferrorhodonite series

The most common minerals in manganese mineralization at the Prakovce–Zimná Voda were identified as rhodonite-group minerals with general structural formula $^{\mathrm{VII}}M(5)^{\mathrm{VI}}M(1)^{\mathrm{VI}}M(2)^{\mathrm{VI}}M(3)^{\mathrm{VI}}M(4)$ [$\mathrm{Si_5O_{15}}$] (Shchipalkina et al. 2019). Identified minerals are rhodonite ($\mathrm{CaMn^3Mn[Si_5O_{15}]}$), which continuously transits into the Fe-rich rhodonite or ferrorhodonite ($\mathrm{CaMn_3Fe[Si_5O_{15}]}$), occurring dominantly in the form of anhedral to subhedral grains up to 0.3 mm in size, grouped to the massive aggregates (Fig. 3a). Macroscopically they cannot be distinguished as they form fine-grained pink masses of a solid solution between both end-members. Moreover, rhodonite-ferrorhodonite series form partially terminated crystals 0.2 mm in size on the edges of cavities filled mainly by quartz or carbonate minerals (Fig. 3b). In BSE images, no visible zoning in rhodonite-ferrorhodonite masses was observed. They are associated dominantly with magnetite, quartz, Mn-carbonates, spessartine and andradite.

Tab. 1 Average chemical composition (in wt. %) and corresponding calculated empirical formulae of magnetite, pyroxenoids, rhodochrosite, kutnohorite, spessartine, andradite, clino-suenoite and clino-ferro-suenoite from Prakovce–Zimná Voda manganese occurrence

Mineral	Magnetite		Rhodonite	Ferro-rhodonite	Kutnohorite		Rhodochrosite		Spessartine	Andradite	Clino-suenoite	Clino-ferro-suenoite	Fluor-apatite
Localization	Magnetite ore	Manganese ore	matrix	matrix	matrix	vein	matrix	vein	matrix	matrix	vein	vein	matrix
Number of analyses (n)	4	10	9	54	10	15	10	10	76	32	9	38	15
P_2O_5	–	–	–	–	–	–	–	–	–	–	–	–	40.84
SiO_2	0.10	0.13	45.88	45.88	0.00	0.00	0.00	0.00	35.19	34.34	52.20	51.14	0.28
TiO_2	0.07	0.02	0.03	0.02	–	–	–	–	0.06	0.01	0.01	0.01	0.03
Al_2O_3	0.00	0.02	0.01	0.02	0.00	0.00	0.00	0.00	16.24	0.80	0.05	0.04	0.04
V_2O_3	0.02	0.01	0.01	0.01	–	–	–	–	0.02	0.02	0.00	0.01	–
Cr_2O_3	0.01	0.00	0.01	0.01	–	–	–	–	0.01	0.01	0.00	0.01	–
Y_2O_3	–	–	–	–	–	–	–	–	0.02	0.02	–	–	0.02
As_2O_3	–	–	–	–	–	–	–	–	–	–	–	–	0.69
REE*	–	–	–	–	–	–	–	–	–	–	–	–	0.06
Fe_2O_3**	68.82	67.31	–	–	–	–	–	–	8.39	32.47	0.68	0.79	–
FeO	30.78	30.42	5.70	7.95	2.66	1.54	0.91	0.93	0.79	0.13	18.27	21.64	0.21
MnO	0.01	0.00	42.62	39.99	25.74	24.53	46.08	50.06	32.57	6.59	15.99	17.30	0.88
MgO	0.01	0.00	0.44	0.65	0.62	0.41	0.42	0.59	0.04	0.04	10.64	7.54	0.02
CoO	0.12	0.09	–	–	–	–	–	–	–	–	0.03	0.04	–
NiO	0.01	0.00	0.01	0.01	–	–	–	–	0.00	0.00	0.05	0.04	–
ZnO	0.03	0.00	0.00	0.00	0.02	0.02	0.03	0.02	0.04	0.05	0.06	0.05	–
BaO	–	–	–	–	0.01	0.01	0.01	0.00	–	–	0.00	0.00	0.06
SrO	–	–	–	–	0.07	0.025	0.02	0.03	–	–	–	–	0.10
CaO	–	–	6.11	5.84	29.13	31.54	13.17	9.32	6.77	27.19	0.75	0.52	54.17
Na_2O	–	–	0.00	0.00	0.01	0.01	0.00	0.01	0.01	0.01	0.02	0.04	0.00
K_2O	–	–	0.00	0.00	0.00	0.00	0.00	0.00	0.01	0.00	0.00	0.00	0.00
H_2O***	–	–	–	–	–	–	–	–	–	–	1.90	1.88	0.00
F	–	–	–	–	–	–	–	–	–	–	0.14	0.11	3.95
Cl	–	–	–	–	–	–	–	–	–	–	0.00	0.00	0.00
O=F,Cl	–	–	–	–	–	–	–	–	–	–	–0.06	–0.05	–1.66
CO_2****	–	–	–	–	41.19	41.48	39.96	39.63	–	–	–	–	–
Total	100.35	98.15	100.83	100.36	99.46	99.77	100.60	100.60	100.15	99.74	100.75	101.10	101.35
P	–	–	–	–	–	–	–	–	–	–	–	–	2.966
Si	0.004	0.005	4.918	4.930	0.000	0.000	0.000	0.000	2.911	2.909	7.956	7.949	0.025
Al	0.000	0.001	0.002	0.003	0.000	0.000	0.000	0.000	1.582	0.101	0.010	0.007	0.004
Ti	0.002	0.001	0.003	0.001	–	–	–	–	0.004	0.001	0.001	0.001	0.002
As	–	–	–	–	–	–	–	–	–	–	–	–	0.036
REE*	–	–	–	–	–	–	–	–	–	–	–	–	0.002
Fe^{3+}	1.987	1.987	–	–	–	–	–	–	0.555	2.009	0.078	0.092	–
V	0.001	0.000	0.001	0.000	–	–	–	–	0.001	0.001	0.000	0.001	–
Cr	0.000	0.000	0.001	0.001	–	–	–	–	0.001	0.001	0.000	0.001	–
Y	–	–	–	–	–	–	–	–	0.001	0.001	–	–	0.001
Fe^{2+}	0.988	0.998	0.511	0.714	0.040	0.023	0.014	0.014	0.055	0.009	2.329	2.818	0.015
Mg	0.001	0.000	0.070	0.103	0.017	0.011	0.011	0.016	0.005	0.004	2.417	1.741	0.002
Mn	0.013	0.004	3.869	3.640	0.388	0.367	0.715	0.784	2.281	0.476	2.064	2.280	0.063
Co	0.004	0.003	–	–	–	–	–	–	–	–	0.004	0.005	–
Ni	0.000	0.000	0.001	0.001	–	–	–	–	0.000	0.000	0.006	0.005	–
Zn	0.001	0.000	0.000	0.000	0.000	0.000	0.000	0.000	0.002	0.003	0.007	0.006	–
Ca	–	–	0.702	0.672	0.555	0.597	0.256	0.185	0.600	2.484	0.123	0.087	4.905
Ba	–	–	–	–	0.000	0.000	0.000	0.000	–	–	0.000	0.000	0.002
Sr	–	–	–	–	0.001	0.003	0.000	0.000	–	–	–	–	0.005
Na	–	–	0.000	0.000	0.000	0.000	0.000	0.000	0.001	0.001	0.005	0.012	0.000
K	–	–	0.000	0.000	0.000	0.000	0.000	0.000	0.001	0.000	0.001	0.001	0.000
OH	–	–	–	–	–	–	–	–	–	–	1.933	1.947	0.001
F	–	–	–	–	–	–	–	–	–	–	0.066	0.053	0.998
Cl	–	–	–	–	–	–	–	–	–	–	0.001	0.001	0.000
Total cat.	3.000	3.000	10.077	10.066	1.000	1.000	1.000	1.000	8.000	8.000	15.001	15.005	5.035
Total an.	–	–	15.000	15.000	–	–	–	–	–	–	2.000	2.000	1.000

Chemical formulae of pyroxenoids calculated on the basis of 15 O atom (*apfu*), magnetite on the basis of 3 cations (*apfu*), carbonates on the basis of 1 cation (*apfu*), garnets and fluorapatite on the basis of 8 cations (*apfu*), amphiboles on the basis of 15 cations (*apfu*) with $(OH)^-$ calculated as F + OH + Cl = 2 anions (*apfu*). Symbols: * REE: sum $La_2O_3 + Ce_2O_3 + Pr_2O_3 + Nd_2O_3 + Sm_2O_3$ and sum of their *apfu*, respectively, ** – calculation of Fe_2O_3 from charge balance, *** – calculation of H_2O from $(OH)^-$, **** – calculation of CO_2.

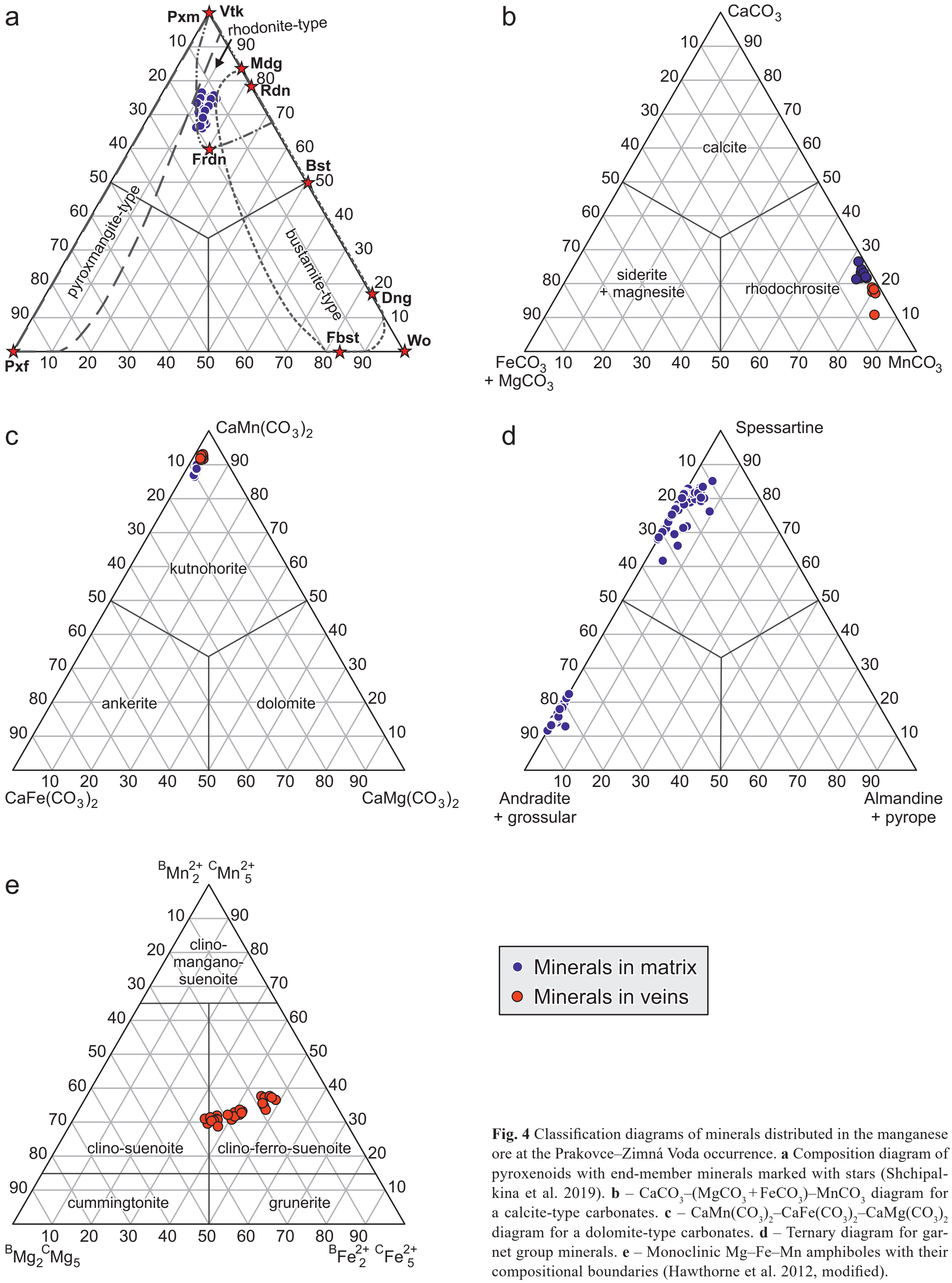

Fig. 4 Classification diagrams of minerals distributed in the manganese ore at the Prakovce–Zimná Voda occurrence. **a** Composition diagram of pyroxenoids with end-member minerals marked with stars (Shchipalkina et al. 2019). **b** – $CaCO_3$–($MgCO_3$+$FeCO_3$)–$MnCO_3$ diagram for a calcite-type carbonates. **c** – $CaMn(CO_3)_2$–$CaFe(CO_3)_2$–$CaMg(CO_3)_2$ diagram for a dolomite-type carbonates. **d** – Ternary diagram for garnet group minerals. **e** – Monoclinic Mg–Fe–Mn amphiboles with their compositional boundaries (Hawthorne et al. 2012, modified).

Chemical composition of the pyroxenoids is shown in a classification diagram (Fig. 4a), which displays good agreement of studied samples with the rhodonite-type structure. Rhodonite-type structure was also verified by X-ray diffraction analysis in order to differentiate pyroxmangite-type structure. Minerals are Ca dominant at the *M*5 site with ^{M5}Ca/(Ca+Mn) ratio in the range 0.51–0.81. If sites *M*1, *M*2 and *M*3 are fully occupied by Mn, the Mn/(Mn+Fe) ratio at the crystallochemical position *M*4 shows range 0.11–0.55 and thus corresponds to ferrorhodonite (<0.5) and minor rhodonite (>0.5) (Shchipalkina et al. 2019). Content of $^{M4}Fe^{2+}$ in rhodonite-ferrorhodonite series was observed up to 0.91 *apfu* (Tab. 1, ESM1). Minerals of rhodonite-ferrorhodonite series show slightly elevated content of Mg (up to 0.16 *apfu*) and Ni (up to 0.01 *apfu*).

4.2.3. Carbonates

Carbonates frequently occurring in manganese were identified as rhodochrosite and kutnohorite. Both carbonates associate with rhodonite–ferrorhodonite series and garnets in the matrix or crystalize in rhodonite cavities (Fig. 3b). More extensively they form rhodochrosite- or kutnohorite-rich veins alongside with quartz, amphiboles and baryte. Accumulations of carbonates (mainly rhodochrosite) form light pink masses, veins with carbonates are white to light pink colour reaching size up to 0.5 cm.

Chemical composition of rhodochrosite I (Fig. 4b) from matrix shows dominant $MnCO_3$ molecule (69.9–76.5 mol. %) with high content of $CaCO_3$ molecule (up to 26.4 mol. %) and relatively low content of Fe^{2+} (up to 0.03 *apfu*) and Mg (up to 0.02 *apfu*). Compared to rhodochrosite II from veins, rhodochrosite shows slightly elevated content of $MnCO_3$ (79.8–84.0 mol. %) and decreased $CaCO_3$ (10.8–18.8 mol. %) molecules with similar contents of Fe^{2+} (up to 0.03 *apfu*) and Mg (0.03 *apfu*).

Chemical analyses of kutnohorite I (Fig. 4c) from matrix show, except for stable content of $MnCO_3$ (39.8–43.6 mol. %) and $CaCO_3$ (50.7–55.6 mol. %), a significant elevation in $FeCO_3$ (up to 5 mol. %) and $MgCO_3$ (up to 1.5 mol. %) molecules. In comparison with kutnohorite II from vein-type samples, contents of $MnCO_3$ (38.0–42.2 mol. %), $CaCO_3$ (53.6–59.0 mol. %) and $MgCO_3$ (up to 1.2 mol. %) molecules are relatively similar, the $FeCO_3$ (2.0–3.2 mol. %) molecule is significantly lower. The substitution diagrams for kutnohorite reveal a good correlation between Mn, Fe and Mg (Fig. 4c). Moreover, the content of SrO in vein-type kutnohorite II is up to 0.4 wt. %, what subtly exceeds content in kutnohorite I from matrix (up to 0. 1 wt. %).

4.2.4. Garnet supergroup minerals

Garnets are one of the common minerals identified in the manganese ore, occurring in the form of yellow to light orange aggregates in the pinkish rhodonite mass. Depending on environment of their occurrence, chemical composition and morphological shapes, garnets can be divided into two types.

The first type is characterized by dominant spessartine component and is associated mostly with rhodonite–ferrorhodonite series, rhodochrosite, kutnohorite and quartz. Spessartine forms subhedral crystals up to 100 μm in size, mostly grouped to the bigger aggregates reaching approximately 0.5 mm in size. Spessartine shows no chemical zoning in BSE imaging, it is mostly cut by system of younger rhodochrosite, kutnohorite and amphibole veins (Fig. 3b). Chemical composition of studied samples (Fig. 4d) varies with dominant spessartine molecule (61.5–85.1 mol. %), elevated and variable andradite molecule (9.5–33.8 mol. %) and elevated almandine molecule (up to 7.4 mol. %) (Tab. 1).

The second type is represented by dominance of andradite. Crystals in the central parts are often porous with a system of multidirectional internal fissures (Fig. 3c), caused by dissolution of more unstable internal parts. Andradite garnets reach size up to 2.5 mm, macroscopically they form light green anhedral to euhedral crystals grouped to the bigger masses. A more detailed view in BSE imaging of selected porous crystals shows tens of small garnet crystals overgrowing an older, almost completely corroded spessartine (Fig. 3d). The outer parts of andradite garnets have a circular cross-section of an irregular shape. The central and porous parts of garnets contain quartz. Locally, internal parts of andradite garnets contain irregularly shaped relicts of spessartine (Fig. 3d). Porous andradite garnets with complete lack of residual spessartine can be observed rather rarely, these crystals reach size up to 10 μm (Fig. 3e). The chemical composition of porous garnets shows (Fig. 4d) dominance of andradite (77.0–88.2 mol. %) with elevated spessartine molecule (11.6–22.7 mol. %) and slightly higher almandine molecule (up to 3.9 wt. %) with minimal content of other components.

4.2.5. Amphibole supergroup minerals

Minerals of the amphibole supergroup with general formula $AB_2C_5T_8O_{22}W_2$ (Hawthorne et al. 2012) at the locality Prakovce are represented by clino-suenoite (ideally $\square Mn^{2+}_2Mg_5Si_8O_{22}(OH)_2$) and clino-ferro-suenoite (ideally $\square Mn^{2+}_2Fe^{2+}_5Si_8O_{22}(OH)_2$) (Oberti et al. 2018). Amphiboles form light to dark green acicular aggregates up to 1 cm in size composed of elongated flattened crystals. Amphiboles mostly occur in the veins cutting the rhodonite–ferrorhodonite–quartz matrix associated with carbonates, frequently occurring in the manganese ore cavities. In BSE imaging they show significant zoning reflecting a change in chemical composition with lighter parts composed dominantly of clino-ferro-suenoite and darker parts consisting of clino-suenoite (Fig. 3f).

The chemical composition of amphiboles is shown in classification diagram (Fig. 4e) indicating linear substitution trend between Mg and Fe^{2+} at the crystallochemical positions *B* and *C*. Clino-suenoite at the position *A* is dominantly vacant with minor Na and K content. The *B* site mostly consists of Mn (around 1.8 *apfu*) with minor Ca (up to 0.17 *apfu*) and very small amount of Na (up to 0.01 *apfu*). At the position *C* content of Mg (2.38–2.45 *apfu*) prevails over Fe^{2+} (2.27–2.38 *apfu*) with relatively high Mn (0.13–0.27 *apfu*) with minimum Fe^{3+}, Zn, Ni and Co values. Anion position *W* is mostly composed of $(OH)^-$ with minor F^- (up to 0.21 *apfu*).

The chemical composition of clino-ferro-suenoite is characterized by a significantly higher content of Fe^{2+} (2.37–3.34 *apfu*) compared to Mg (1.00–2.34 *apfu*), with an increase in Mn content (up to 0.82 *apfu*) at the position *C*. A larger number of clino-ferro-suenoite analyses shows elevated Mn content at the both *B* (1.86–1.95 *apfu*) and *C* (0.11–0.82 *apfu*) positions, which is reflected by a slight shift of the analyses toward the hypothetical *clino-mangano-suneoite* field (Fig. 4e). Contents of other components at all other crystallochemical positions are similar to those in clino-suenoite.

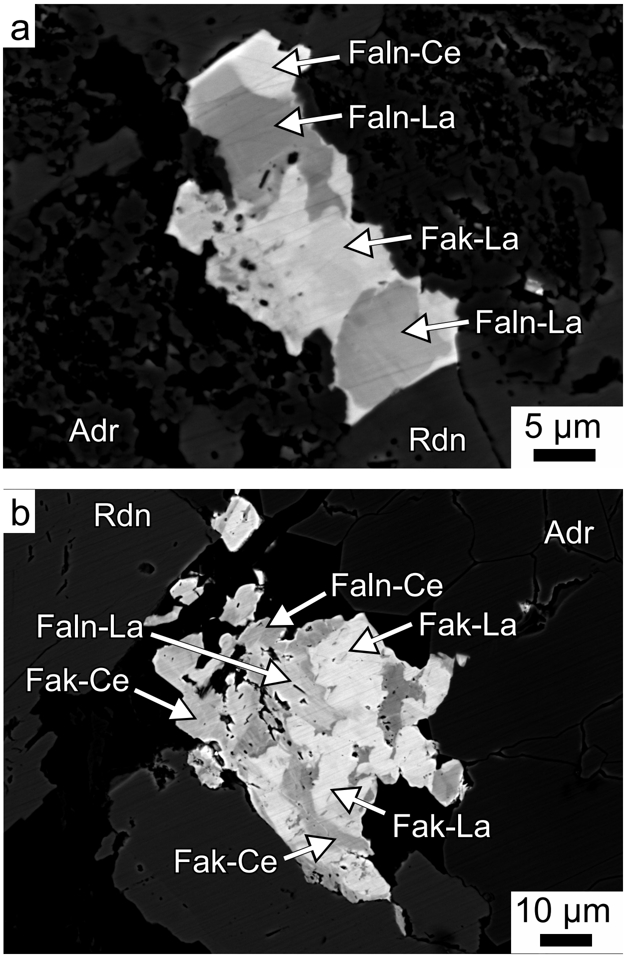

Fig. 5: BSE images of epidote supergroup minerals associated with andradite in rhodonite matrix. **a** – Strongly zonal crystals. **b** – Polycrystalline aggregates.

4.2.6. Epidote-group minerals

Epidote-group minerals from Prakovce were identified as members of allanite-subgroup, namely ferriallanite-(La), ferriallanite-(Ce), ferriakasakaite-(La) and ferriakasakaite-(Ce). They occur as rare interstitial phases within rhodonite-ferrorhodonite series aggregates, dominantly in association with andradite. The aggregates show dark brown colour, distinguishing of particular species based on macroscopic appearance is impossible. Their grains in BSE imaging form strongly zonal anhedral crystals (Fig. 5a) or zonal polycrystalline aggregates (Fig. 5b), indicated by the presence of different shades of grey colour in these domains. Size of the studied aggregates reaches up to 50 µm in size.

Minerals of ferriakasakaite series form the most common constituents in zonal allanite-subgroup polycrystalline aggregates, where they form small crystals or narrow thin strips. Minerals form a solid-solution and their crystallochemical position *M*3 is dominantly occupied by Mn^{2+} (0.39–0.55 *apfu*) over Fe^{2+} (0.13–0.40 *apfu*), the *M*1 position dominantly contains calculated Fe^{3+} (0.94–1.25 *apfu*). The content of $Y+REE^{3+}$ varies between 0.70–0.97 *apfu.* The dominant La^{3+} content (up to 0.47 *apfu*) and minor Ce^{3+} (up to 0.34 *apfu*) is present in ferriakasakaite-(La) and the dominant content of Ce^{3+} (0.32 *apfu*) over La^{3+} (0.31 *apfu*) was observed in ferriakasakaite-(Ce) (Tab. 2). Minerals of ferriakasakaite series show occupancy of position A in a ratio of approximately 1 : 3 (Ca vs Mn), what indicates participation of ferriandrosite component.

Minerals of ferriallanite series occur less often in the form of small zones or anhedral crystals in allanite-subgroup polycrystalline aggregates. Minerals of ferriallanite series at the crystallochemical position *M*3 dominantly contain Fe^{2+} (0.37–0.54 *apfu*) over Mn^{2+} (0.28–0.34 *apfu*), the *M*1 position dominantly contains calculated Fe^{3+} (0.86–1.03 *apfu*). Their content of $Y+REE^{3+}$ is in the range 0.73–0.90 *apfu,* where ferriallanite-(La) at the *A*2 position dominantly contains La^{3+} (up to 0.39 *apfu*) over Ce^{3+} (0.27–0.34 *apfu),* whereas ferriallanite-(Ce) dominantly consists of Ce^{3+} (up to 0.40 *apfu*) over La^{3+} (0.29–0.37 *apfu*). Both minerals show elevated content of Nd^{3+} (up to 0.14 *apfu*) and Pr^{3+} (up to 0.05 *apfu*) (Tab. 2).

4.2.7. Fluorapatite

Fluorapatite is a relatively common mineral in manganese ore, it forms accumulations up to 100 µm in size

Tab. 2 Quantitative chemical analyses (in wt. %) and corresponding calculated empirical formulae of epidote supergroup from Prakovce–Zimná Voda manganese occurrence

Mineral	Ferriallanite-(La)					Ferriallanite-(Ce)		Ferriakasakaite-(La)						Ferriakasakaite-(Ce)
Analysis	1	2	3	4	5	1	2	1	2	3	4	5	6	1
SiO_2	28.90	28.77	29.77	29.33	29.04	28.59	29.62	30.08	28.23	28.58	28.04	29.63	28.66	29.65
TiO_2	0.53	1.23	1.30	1.44	0.13	0.91	0.19	0.29	0.95	1.05	1.13	0.33	0.52	0.19
ThO_2	0.00	0.06	0.13	0.15	0.00	0.28	0.07	0.08	0.11	0.11	0.00	0.00	0.00	0.08
Al_2O_3	11.47	10.15	11.15	10.68	11.76	9.43	13.03	9.56	9.22	9.33	10.11	10.55	9.38	11.30
V_2O_3	0.42	0.19	0.32	0.45	0.19	0.29	0.17	0.06	0.09	0.00	0.34	0.00	0.16	0.17
Cr_2O_3	0.03	0.00	0.09	0.02	0.00	0.09	0.08	0.00	0.09	0.00	0.00	0.00	0.04	0.00
Y_2O_3	0.00	0.00	0.13	0.00	0.00	0.00	0.00	0.00	0.00	0.00	0.00	0.00	0.00	0.00
La_2O_3	10.62	9.54	7.40	8.04	9.70	9.83	7.95	8.87	12.39	12.23	9.66	8.93	12.00	8.49
Ce_2O_3	9.16	8.84	7.08	7.25	9.09	10.85	8.38	7.00	8.80	8.79	9.31	7.11	8.89	8.78
Pr_2O_3	1.30	1.16	1.25	1.08	1.29	0.96	1.19	0.91	1.25	1.25	1.03	1.04	1.34	1.18
Nd_2O_3	3.07	3.40	3.94	3.63	3.06	2.02	3.43	2.40	2.94	2.97	2.89	2.58	2.82	3.26
Sm_2O_3	0.00	0.00	0.18	0.13	0.17	0.04	0.06	0.08	0.00	0.00	0.00	0.00	0.00	0.00
Eu_2O_3	0.31	0.29	0.30	0.35	0.29	0.09	0.30	0.10	0.34	0.37	0.29	0.20	0.32	0.28
Gd_2O_3	0.00	0.00	0.08	0.00	0.00	0.00	0.05	0.00	0.06	0.00	0.18	0.08	0.06	0.00
Dy_2O_3	0.00	0.09	0.05	0.00	0.00	0.00	0.05	0.00	0.00	0.00	0.05	0.00	0.06	0.00
Ho_2O_3	0.00	0.21	0.00	0.06	0.00	0.00	0.06	0.00	0.00	0.14	0.00	0.00	0.00	0.15
Er_2O_3	0.10	0.00	0.06	0.00	0.00	0.10	0.11	0.15	0.07	0.00	0.09	0.00	0.00	0.10
Fe_2O_3*	11.49	12.65	13.09	14.07	13.63	13.13	12.90	16.96	12.37	11.43	14.26	16.86	12.22	13.91
FeO	5.89	5.84	5.08	4.84	4.91	6.20	4.46	1.58	4.18	4.54	3.93	1,95	4.51	4.05
MgO	0.19	0.12	0.13	0.22	0.20	0.00	0.12	0.20	0.29	0.29	0.10	0.15	0.27	0.19
MnO	6.79	6.07	5.58	5.66	6.31	7.42	6.25	10.66	9.83	10.30	7.43	8.93	9.06	7.81
CaO	7.77	8.87	10.54	10.26	8.64	7.37	9.54	8.81	6.44	6.17	8.60	9.55	6.93	8.69
PbO	0.00	0.04	0.00	0.00	0.00	0.00	0.07	0.00	0.10	0.06	0.10	0.00	0.06	0.00
H_2O**	1.50	1.49	1.54	1.53	1.52	1.48	1.54	1.53	1.46	1.46	1.49	1.54	1.46	1.53
F	0.13	0.03	0.11	0.00	0.00	0.02	0.00	0.06	0.00	0.00	0.07	0.00	0.00	0.00
Cl	0.00	0.00	0.04	0.00	0.00	0.00	0.00	0.00	0.00	0.00	0.01	0.00	0.00	0.00
O=F,Cl	–0.05	–0.01	–0.06	0.00	0.00	–0.01	0.00	–0.02	0.00	0.00	–0.03	0.00	0.00	0.00
Total	99.63	99.02	99.28	99.21	99.91	99.07	99.64	99.35	99.19	99.08	99.07	99.42	98.75	99.81
Si	2.887	2.890	2.903	2.873	2.867	2.905	2.877	2.949	2.898	2.931	2.826	2.893	2.937	2.913
^{IV}Al	0.113	0.110	0.097	0.127	0.133	0.095	0.123	0.051	0.102	0.069	0.174	0.107	0.063	0.087
Total *T*	3.000	3.000	3.000	3.000	3.000	3.000	3.000	3.000	3.000	3.000	3.000	3.000	3.000	3.000
Ti	0.040	0.093	0.095	0.106	0.010	0.069	0.014	0.022	0.074	0.081	0.086	0.024	0.040	0.014
^{VI}Al	1.237	1.091	1.185	1.105	1.235	1.034	1.367	1.053	1.014	1.058	1.026	1.107	1.069	1.221
Cr	0.002	0.000	0.007	0.002	0.000	0.007	0.006	0.000	0.007	0.000	0.000	0.000	0.003	0.000
V	0.034	0.016	0.025	0.035	0.015	0.023	0.013	0.005	0.007	0.000	0.027	0.000	0.013	0.014
Fe^{3+}	0.864	0.953	0.955	1.030	1.013	0.991	0.940	1.247	0.951	0.877	1.081	1.239	0.942	1.024
Fe^{2+}	0.492	0.494	0.420	0.403	0.406	0.540	0.365	0.133	0.364	0.395	0.331	0.159	0.387	0.336
Mg	0.029	0.018	0.019	0.032	0.030	0.000	0.017	0.029	0.045	0.045	0.015	0.022	0.041	0.028
Mn	0.303	0.336	0.294	0.286	0.292	0.336	0.278	0.511	0.539	0.545	0.433	0.449	0.504	0.363
Total *M*	3.000	3.000	3.000	3.000	3.000	3.000	3.000	3.000	3.000	3.000	3.000	3.000	3.000	3.000
Mn	0.272	0.181	0.166	0.184	0.235	0.303	0.236	0.374	0.316	0.350	0.201	0.289	0.282	0.287
Ca	0.831	0.955	1.104	1.077	0.914	0.802	0.996	0.925	0.708	0.680	0.931	0.999	0.761	0.914
Pb	0.000	0.001	0.000	0.000	0.000	0.000	0.002	0.000	0.003	0.002	0.003	0.000	0.002	0.000
La	0.391	0.353	0.266	0.290	0.353	0.369	0.285	0.321	0.469	0.463	0.359	0.321	0.454	0.308
Ce	0.335	0.325	0.253	0.260	0.329	0.404	0.298	0.251	0.331	0.330	0.344	0.254	0.334	0.316
Pr	0.047	0.043	0.044	0.038	0.046	0.035	0.042	0.033	0.047	0.047	0.038	0.037	0.050	0.042
Nd	0.110	0.122	0.137	0.127	0.108	0.073	0.119	0.084	0.108	0.109	0.104	0.090	0.103	0.114
Sm	0.000	0.000	0.006	0.005	0.006	0.002	0.002	0.003	0.000	0.000	0.000	0.000	0.000	0.000
Eu	0.011	0.010	0.010	0.012	0.010	0.003	0.010	0.003	0.012	0.013	0.010	0.007	0.011	0.010
Gd	0.000	0.000	0.003	0.000	0.000	0.000	0.002	0.000	0.002	0.000	0.006	0.003	0.002	0.000
Dy	0.000	0.003	0.002	0.000	0.000	0.000	0.002	0.000	0.000	0.000	0.002	0.000	0.002	0.000
Ho	0.000	0.007	0.000	0.002	0.000	0.000	0.002	0.000	0.000	0.005	0.000	0.000	0.000	0.005
Er	0.003	0.000	0.002	0.000	0.000	0.003	0.003	0.005	0.002	0.000	0.003	0.000	0.000	0.003
Th	0.000	0.001	0.003	0.003	0.000	0.007	0.002	0.002	0.003	0.003	0.000	0.000	0.000	0.002
Total *A*	2.000	2.000	2.000	2.000	2.000	2.000	2.000	2.000	2.000	2.000	2.000	2.000	2.000	2.000
Total REE	0.897	0.862	0.727	0.736	0.851	0.889	0.764	0.699	0.970	0.966	0.865	0.712	0.955	0.797
F^-	0.040	0.010	0.035	0.000	0.000	0.006	0.000	0.018	0.000	0.000	0.023	0.000	0.000	0.000
Cl^-	0.000	0.000	0.006	0.000	0.000	0.000	0.000	0.000	0.000	0.000	0.001	0.000	0.000	0.000
O^{2-}	23.960	23.990	23.959	24.000	24.000	23.994	24.000	23.982	24.000	24.000	23.975	24.000	24.000	24.000
Total *O4*	24.000	24.000	24.000	24.000	24.000	24.000	24.000	24.000	24.000	24.000	24.000	24.000	24.000	24.000
OH^-	1.000	1.000	1.000	1.000	1.000	1.000	1.000	1.000	1.000	1.000	1.000	1.000	1.000	1.000
Total *O10*	1.000	1.000	1.000	1.000	1.000	1.000	1.000	1.000	1.000	1.000	1.000	1.000	1.000	1.000

Chemical formulae calculated on the basis of (A+M+T)=8 cations (*apfu*), symbol * represents calculation of Fe_2O_3 from the charge balance of the molecule, symbol ** represents calculation of H_2O from $(OH)^-$.

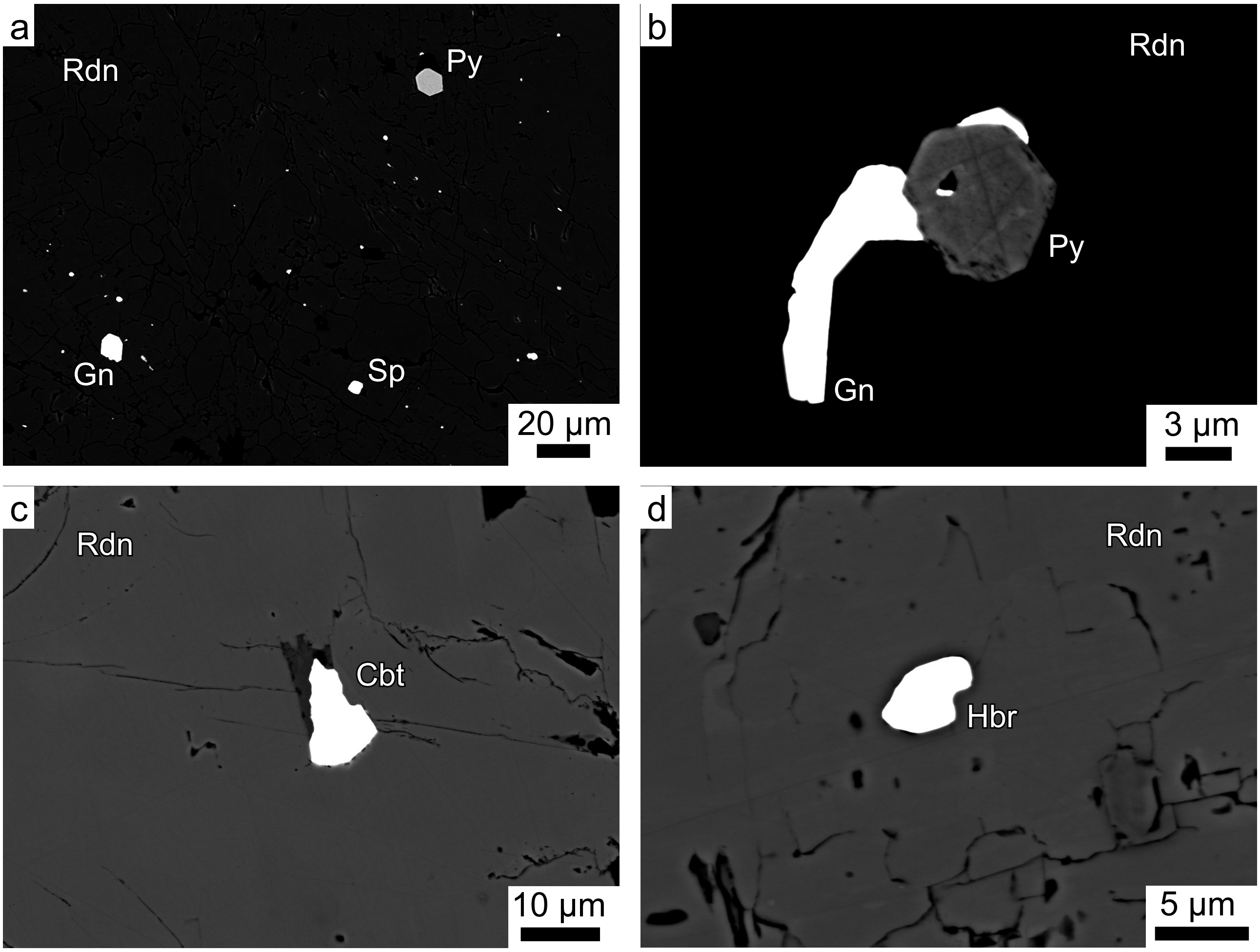

Fig. 6 BSE images of sulfidic mineralization and hübnerite. **a** – Distribution of galena, sphalerite and pyrite grains in rhodonite matrix. **b** – Euhedral crystal of pyrite associated with galena. **c** – Cobaltite grain in rhodonite vug. **d** – Hübnerite grain in rhodonite.

consisting of subhedral grains embedded in rhodochrosite, to a lesser content it was also observed to be cut by kutnohorite veins associated with spessartine (Fig. 3g). Chemical composition of fluorapatite is homogenous. Some analyses show elevated contents of As_2O_5 up to 3.1 wt. %, what corresponds to 0.14 *apfu* As^{5+}. Fluorapatite contains elevated content of Mn^{2+} (up to 0.16 *apfu*) and Fe^{2+} (up to 0.05 *apfu*). Content of Y+REE is low (on average 0.1 wt. %; 0.02 *apfu* respectively). The anion site is dominantly occupied by F^- (0.98–1.00 *apfu*) with minimal Cl^- or $(OH)^-$ anions (Tab. 1).

4.2.8. Baryte

Baryte represents a rare mineral, which occurs in the form of isolated anhedral grains up to 30 μm in size dominantly in association with rhodochrosite and kutnohorite veins (Fig. 3h) or in the interstitial spaces between rhodonite crystals. In baryte, elevated content of Mn (0.04–0.05 *apfu*) was observed, together with up to 0.03 *apfu* Fe^{2+}, 0.02 *apfu* Al^{3+} and 0.01 *apfu* Na (ESM1).

4.2.9. Sulfide minerals

Sulfides are relatively rare at the studied locality and are represented by *galena*, *sphalerite*, *pyrite* and *cobaltite* which are embedded in cavities of rhodonite–ferrorhodonite matrix. They dominantly form anhedral grains up to 10 μm in size (Fig.6a). Only pyrite was locally observed in the form of subhedral to euhedral grains (Fig. 6a, b). Cobaltite was identified rarely only in one anhedral grain with no visible zoning in BSE (Fig. 6c). Chemical composition of sulfides is monotonous with formulae close to ideal end-members (Tab. 3). The only exception is cobaltite with significantly elevated content of Ni (0.21–0.32 *apfu*). A slightly elevated content of Mn was observed in all sulfides, namely in cobaltite (up to 0.09 *apfu*), galena (up to 0.08 *apfu*), sphalerite (up to 0.05 *apfu*) and pyrite (up to 0.04 *apfu*) (Tab. 3).

4.2.10. Hübnerite

Hübnerite occurs rarely and it was identified only in one sample as a subhedral grain up to 5 μm in size (Fig. 6d).

Tab. 3 Quantitative chemical analyses (in wt. %) and corresponding calculated empirical formulae of pyrite, galena, sphalerite and cobaltite from Prakovce–Zimná Voda manganese occurrence

Mineral	Sphalerite		Galena				Pyrite			Cobaltite				
Analysis	1	2	1	2	3	4	1	2	3	1	2	3	4	5
Pb	–	–	84.22	84.14	83.45	82.80	–	–	–	–	–	–	–	–
Ag	–	–	0.35	0.27	0.34	0.32	–	–	–	–	–	–	–	–
Cu	0.00	0.00	0.08	0.10	0.07	0.00	0.00	0.00	0.00	0.00	0.00	0.00	0.00	0.00
Fe	0.38	0.40	0.02	0.23	0.04	0.43	43.62	41.79	43.61	3.05	3.05	4.24	4.87	4.64
Co	–	–	–	–	–	–	0.09	1.32	0.23	24.79	23.66	19.24	19.39	18.79
Ni	–	–	–	–	–	–	0.00	0.16	0.17	7.30	8.43	11.47	10.28	11.29
Zn	64.58	64.15	–	–	–	–	–	–	–	–	–	–	–	–
Cd	0.05	0.13	–	–	–	–	–	–	–	–	–	–	–	–
Mn	2.70	2.52	0.69	1.00	0.63	1.76	0.78	1.82	1.13	1.99	2.00	2.75	2.89	2.68
Bi	–	–	1.21	1.11	1.25	1.26	0.46	0.00	0.00	0.00	0.00	0.86	0.00	0.00
As	–	–	0.00	0.00	0.00	0.00	0.00	1.38	0.17	44.51	44.20	43.26	43.68	43.32
S	33.53	33.30	12.91	13.04	12.90	12.22	53.97	52.00	54.73	18.30	18.40	18.77	19.26	18.95
Total	101.24	100.50	99.47	99.89	98.67	98.79	98.92	98.46	100.03	99.93	99.75	100.59	100.37	99.66
Pb	–	–	0.977	0.962	0.974	0.964	–	–	–	–	–	–	–	–
Ag	–	–	0.008	0.006	0.008	0.007	–	–	–	–	–	–	–	–
Cu	0.000	0.000	0.003	0.004	0.003	0.000	0.000	0.000	0.000	0.000	0.000	0.000	0.000	0.000
Fe	0.006	0.007	0.001	0.010	0.002	0.019	0.944	0.917	0.931	0.091	0.091	0.126	0.143	0.138
Co	–	–	–	–	–	–	0.002	0.027	0.005	0.701	0.669	0.540	0.540	0.528
Ni	–	–	–	–	–	–	0.000	0.003	0.003	0.207	0.239	0.323	0.287	0.318
Zn	0.945	0.946	–	–	–	–	–	–	–	–	–	–	–	–
Cd	0.000	0.001	–	–	–	–	–	–	–	–	–	–	–	–
Mn	0.047	0.044	0.030	0.043	0.028	0.077	0.017	0.041	0.024	0.060	0.061	0.083	0.086	0.081
Bi	–	–	0.014	0.013	0.014	0.015	0.003	0.000	0.000	0.000	0.000	0.007	0.000	0.000
Cat. Sum	0.999	0.998	1.032	1.037	1.028	1.081	0.966	0.989	0.963	1.059	1.060	1.078	1.057	1.065
As	–	–	0.000	0.000	0.000	0.000	0.000	0.023	0.003	0.990	0.983	0.954	0.957	0.957
S	1.001	1.002	0.968	0.963	0.972	0.919	2.034	1.988	2.034	0.951	0.957	0.968	0.986	0.978
An. Sum	1.001	1.002	0.968	0.963	0.972	0.919	2.034	2.011	2.037	1.941	1.940	1.922	1.943	1.935
#Co	–	–	–	–	–	–	–	–	–	0.70	0.67	0.55	0.56	0.54
#Ni	–	–	–	–	–	–	–	–	–	0.21	0.24	0.33	0.30	0.32
#Fe	–	–	–	–	–	–	–	–	–	0.09	0.09	0.13	0.15	0.14

Chemical formulae of sphalerite, galena and pyrite are based on sum of all atoms = 2 *apfu*, cobaltite on sum of all atoms = 3 *apfu.*

The chemical composition shows elevated content of Fe^{2+} (up to 0.05 *apfu*) (ESM1).

5. Discussion

5.1. Chemical composition and classification of rhodonite-group minerals

The nomenclature of the rhodonite group minerals is based on the dominant occupancy of the *M* sites where Ca at *M*5 position gives root-name rhodonite and prefix is used when site $M4 \neq$ Mn, the prefix "ferro" is added when Fe^{2+} dominantly occupies the *M*4 position (Shchipalkina et al. 2019). Thus, following the IMA approved nomenclature rules, the pyroxenoids from Prakovce with ^{M5}Ca/(Ca + Mn) > 0.50 and ^{M4}Mn/(Mn + Fe) > 0.50 (in the range 0.61–0.76 and 0.51–0.55, respectively, Tab. 1, ESM1) are classified as rhodonite and ^{M5}Ca/(Ca + Mn) > 0.50 and ^{M4}Mn/(Mn + Fe) < 0.50 (in the range 0.51–0.81 and 0.11–0.50, respectively, Tab. 1, ESM1) as ferrorhodonite. However, Shchipalkina et al. (2017) based on Mössbauer spectroscopy in ferrorhodonite suggests, that Fe arrangement between *M* sites should be distributed among the *M*4 polyhedron occupying 62.5 ± 2 % Fe and the remaining 37.5 ± 2 % Fe should be divided to *M*1, *M*2 and *M*3 distorted octahedrons. Therefore, it is challenging to consider some analyses without proper crystallochemical measurements as ferrorhodonite and therefore certain minerals described as ferrorhodonite may be Fe-rich rhodonite (ESM1: analyses 42–54).

5.2. Comparison of studied allanite-group minerals with occurrences in the world

Minerals of the epidote supergroup were identified as ferriallanite-(La), ferriallanite-(Ce), ferriakasakaite-(Ce) and ferriakasakaite-(La), all representing allanite group. The structural formula of epidote supergroup minerals is defined as $A1A2M1M2M3(SiO_4)(Si_2O_7)O(OH)$ (Armbruster et al. 2006). The structure of ferriallanite-(Ce) and ferriallanite-(La) consists of dominant Fe^{2+} cation at the octahedral *M*3 position and Fe^{3+} cation at the octahedral *M*1 position. The dominant REE^{3+} cation at the *A*2 site reflects suffix of each end-member. On the other hand, ferriakasakaite-(Ce) and ferriakasakaite-(La) can be defined by dominant Mn^{2+} cation at the octahedral *M3* position with similar cation distribution at the other crystallochemical positions. Site *A*1 is dominantly occupied by Ca^{2+} and octahedral *M*2 position by Al^{3+} in all studied epidotes-supergroup minerals.

Ferriallanite-(Ce) was firstly described from Neprimetnyi peralkaline pegmatite in Ulyn Khuren Mts., Mongolia (Kartashov et al. 2002), since then it was identified at a significant number of localities such as the Bastnäs Fe–Cu–REE deposit in Sweden (Holtstam et al. 2003; Sobek et al. 2023), in alkali-feldspar syenites from Cape Ashizuri in Japan (Nagashima et al. 2011), as a late-stage crystallization product of REE-enriched granitic melt from plagiogranites of the Troodos ophiolite in Cyprus (Anenburg et al. 2015) or in the form of hydrothermal assemblage in peralkaline granites from the Corupá Pluton in Brazil (Vlach 2022). From the Western Carpathian area, ferriallanite-(Ce) was identified in a Permian A-type granite clast from conglomerates embedded in the Cretaceous flysch sequence of the Pieniny Klippen Belt near Stupné, where primary epidotes show significant replacement textures formed during the low-temperature hydrothermal-metamorphic overprint (Uher et al. 2015). Ferriallanite-(La) represents rare mineral identified only at two localities in a void of a Mn-rich sanidinite xenolith in the In den Dellen pumice quarries, Laach Lake volcanic complex, Eifel, Germany (Kolitsch et al. 2012) and in polymineralic nodules containing several REE minerals (e.g. allanite-(Ce), allanite-(La), ferriallanite-(Ce), ferriallanite-(La), bastnäsite-(Ce), bastnäsite-(La) and others) at the gold placer Mochalin Log REE deposit related to the metasomatic contact zone of alkaline intrusive complex in South Urals, Russia (Kasatkin et al. 2020). Minerals of akasakaite series were firstly recommended as possible new members of the allanite subgroup in epidote classification introduced by Armbruster et al. (2006). The first ferriakasakaite-(La) was discovered and approved from an unnamed strata-bound ferromanganese ore deposit in the Shobu area in Japan (Nagashima et al. 2015). Following the before mentioned description, ferriakasakaite-(La) was identified in the eruptive fragments of nosean sanidinite from the In den Dellen Mine near the Laach Lake volcanic complex in Eifel, Germany and from the metasomatic rocks of the Palegonian Massif in Republic of North Macedonia, together with ferriallanite-(La) and ferriallanite-(Ce) (Chukanov et al. 2018; Varlamov et al. 2019). Similarly, ferriakasakaite-(Ce) was firstly approved and subsequently described from the Mn ore deposit of Monte Maniglia, Piedmont in Italy (Biagioni et al. 2019), moreover strongly metamict ferriakasakaite-(Ce) was reported in the hematite-impregnated Mn-silicate rocks at Kesebol in Götaland, Sweden (Bonazzi et al. 2009).

REE-bearing epidotes from the manganese occurrences in the Western Carpathian area were reported only recently from Betliar, occurring in the pyroxmangite veins identified as ferriandrosite-(Ce) and vielleaureite-(Ce) (Myšľan et al. 2023; Števko et al. 2023). In addition, more studies of epidote supergroup minerals from the other manganese deposits are being carried out recently (Girtler et al. 2013; Nagashima et al. 2015; Biagioni et al. 2019 etc.).

5.3. Origin of magnetite–manganese ore at Prakovce occurrence compared to the other Western Carpathian localities

Manganese mineralization in the Spišsko-Gemerské Rudohorie Mts. was generated during the polycyclic development stages of Gemeric Unit. Mn mineralization embedded in the Bystrý Potok Fm. (Gelnica Group) is interpreted to originate from the sedimentary rocks represented by calcareous, argillaceous and terrigenous material, quartz and Ba-rich minerals with material produced by volcanic sources (Rojkovič 2001; Myšľan et al. 2023). Manganese was most probably transported from the deeper anoxic oceanic floors to the shallower oxygen-rich waters allowing the precipitation of manganese oxyhydroxides (Rojkovič 2001) and to some extent influenced by syngenetic basaltic volcanic activity (Kantor 1954; Grecula et al. 1995) accompanied by exhalations of hydrothermal vents. Radvanec and Gonda (2020) assume the formation of Mn mineralization as a result of an anatectic melting of the upper crust generating metasomatic fluids with subsequent Mn-skarn formation. The high content of Fe in manganese ores was interpreted as a consequence of infiltrating volcano-sedimentary fluids of juvenile basaltic volcanism (Ilavský 1957; Grecula et al. 1995). The manganese mineralization at the Diely occurrence near Poráč (Rakovec Group) is assumed to be formed during the back-arc submarine volcanic activity forming the Mn-bearing hydrothermal fluids followed by their precipitation and transformation by later tectono-metamorphic events (Myšľan et al. 2024).

The manganese mineralization at the Zimná Voda occurrence was formed within the magnetite bodies which were generated due to the early Paleozoic bimodal (basalt–rhyloite) volcanic activity, which produced strata-bound Fe-ores hosted in volcano–sedimentary sequences (dominantly composed of rhyolites and their tuffs) of the Drnava Formation (Gelnica Group). The Drnava Formation lacks wide-spread horizons of lydites, metacarbonates and graphitic phyllites; these rocks are present only sporadically in the formation´s uppermost layers (Snopko and Vozárová 1981; Bajaník et al. 1983; Grecula et al. 1995). The lack of metacarbonate bodies at the studied locality causes relative absence of carbonate minerals in the manganese ore hereby mineral composition has predominant silicate character. This trend is opposite compared to the abundant occurrence of metacarbonate lenses in association with manganese mineralization within the Bystrý potok Formation (Ružička et al. 2020; Myšľan and Ružička 2022, etc.). Furthermore, an absence of an organic substrate in the form of metamorphosed graphitic phyllites or lydites at the examined area, compared to the other metamorphosed manganese-bearing localities (Čučma–Čierna baňa, Malá Hekerová–Bystrý potok and Betliar–Július) within the Bystrý potok Formation, illustrates the influence of a different redox conditions during the magnetite–manganese ore formation, emphasizing its oxidic character. Metamorphic processes in greenschist facies conditions affected Fe-bearing deposits during the Variscan and Alpine metamorphic stages via mobilization of elements, their redeposition and accumulation in the suitable porous lithostratigraphic horizons.

Based on the mutual relations between the magnetite bodies and manganese mineralization, we can assume, that magnetite formation represents the oldest mineralization process concurrent with incorporation of a manganese solutions. Magnetite shows no elevated concentration of Mn in the magnetite bodies or in the fragments or isolated grains within the manganese ore (Mn up to 0.01 *apfu*) (Tab. 1, ESM1). Moreover, in some places close to the contact with magnetite ore, magnetite was observed to be replaced by a younger Mn minerals (Fig. 3c). Formation of manganese silicates was related to the high content of Si, Al, Fe and other components in the quartz-rich acidic protolith followed by decarbonisation reactions generating Mn-rich carbonates during the increasing metamorphic conditions.

5.4. Manganese minerals of Variscan metamorphic stage

As the manganese ore is dominantly formed by rhodonite–ferrorhodonite matrix, the low abundance of carbonates (rhodochrosite and kutnohorite) in manganese ore indicates their lack in the protolith as the formation of the most carbonates occurs in the sediment at the early stages of diagenesis (Kuleshov and Maynard 2017). Along with rhodochrosite, fluorapatite occurs (Fig. 3g), what may indicate a contribution of P- and F-rich fluids interacting with the calcium present in the early-formed carbonates.

Spessartine (type 1 garnet) is a common constituent in manganese ore, frequently occurring associated with quartz, carbonates and rhodonite (Fig. 3b). The formation of spessartine is a subject of discussion by several studies (e.g. Hsu 1968; Dasgupta 1997; Nyame 2001; Bataleva et al. 2020). Spessartine in manganiferous assemblages is generated during the metamorphic transformation of precursor manganese oxyhydroxides, siliceous and argillaceous components (Roy 1981). This process is indicated by textural features, the most characteristic of which is the preservation of residual phases due to the imperfect transformation of Mn carbonates or quartz during the prograde growth of spessartine (Nyame 2001). The precursor rocks had a relatively low aluminium content, leading to its nearly complete consumption during the garnet growth. Crystallization of spessartine during the prograde metamorphic events was proved to occur at the low pressure and at temperatures as low as 300 °C (Theye et al. 1996). In some cases (Fig. 3c), the growth of the initial spessartine crystals achieved such a strong crystallization force that caused the displacement of minerals (e.g. magnetite).

5.5. Manganese minerals of Alpine metamorphic stage

At the Prakovce–Zimná Voda occurrence, a significant development of manganese mineralization took place most probably during the Alpine metamorphic event, causing structural deformation indicated by the formation of cracks and fissures, filled by the younger generation of manganese minerals, replacement of existing phases and precipitation of a new minerals from a newly generated hydrothermal solutions with a different chemical composition.

The most notable sign is formation of a system of veins and veinlets dominantly composed by Mn carbonates, amphiboles and baryte alongside with formation of garnets. Baryte was observed only in the interstitial places and veins associated with vein-type carbonates. In association with carbonates, amphibole group minerals were observed forming the vein fillings or accumulations. Clino-suenoite and clino-ferro-suenoite from Prakovce form incomplete substitution series (Fig. 4e). Clino-suenoite was described by Oberti et al. (2018) after modification of amphibole supergroup by Hawthorne et al. (2012), formerly known as manganocummingtonite. The name clino-ferro-suenoite has not been approved yet, however Oberti et al. (2018) stated, that this mineral name should be applied to the amphibole group minerals formerly known as tirodite, dannemorite and manganogrunerite. The temperature estimation in manganese amphiboles is based on the Mn/(Mn+Mg) ratio, forming the wide range of stability limits of clino-suenoite, with 400 °C referring to the lower stability limit at 200 MPa, however iron in the structure of manganese-rich amphiboles reduces their stability limits (Melcher 1995), what corresponds with

P–T conditions of the Alpine metamorphic stage at the temperature 350–460 ºC (e.g. Faryad, 1995).

The one of the most significant features of the manganese ore is the presence of andradite (type 2 garnets) influenced by the fluid infiltration and interaction with spessartine (type 1 garnet). The newly formed type 2 garnets preserve the original shape of the type 1 garnets (Fig. 3c) as evidenced in a more detailed BSE view (Fig. 3d). Based on the observations, the garnet formation processes were caused by dissolution of a type 1 spessartine, mostly affected in the crystal core, which were unstable due to the changes in P–T conditions, further influenced by the formation of cracks. Various researchers have highlighted the significance of the fracture formation during the metamorphic evolution (e.g. Whitney et al. 1996; Konrad-Schmolke et al. 2007; Faryad et al. 2010; Giuntoli et al. 2018) allowing modification of the garnet interior. The newly generated hydrothermal fluids caused resorption of spessartine and release of Mn to the system, allowing formation of other newly-generated Mn-rich phases and garnets with dominant andradite composition (77.0–88.2 mol. %, ESM1), crystallizing around dissolved spessartine (Fig. 3d). Disruption in garnet stoichiometry (*Y* and *X* sites) and Si deficiency in the *T* site (ESM1) might indicate entrance of H_4O_4 into the tetrahedral site what may mean presence of OH-bearing garnet composition (Geiger, Rossman 2020).

The formation of epidotes is related to the low-grade (greenschist facies) Alpine metamorphic event reflecting the high mobility of REE elements. The explanation of the phase occurrence with exceeding La or Ce at the REE^{3+}-dominant *A*2 site reflects the complexity of the processes leading to their formation as well as diverse geochemical signature of the host rocks. For example, Biagioni et al. (2019) states, that the presence of phases dominated by La or Ce can be attributed to multiple factors, for example the early oxidation of Ce to its tetravalent state, what boosts La enrichment among the REE elements, preferentially incorporating Ce in the HREE preferring structures. Similarly, epidote-supergroup minerals from Pelagonian massif contain increased content of La caused by oxidation of Ce^{3+} to Ce^{4+} incorporated into the other, more suitable minerals (Chukanov et al. 2018). Strong zoning in the crystals and formation of zonal polycrystalline aggregates indicates complicated evolution of hydrothermal solutions precipitated during the metamorphic formation of manganese ore. Since the epidotes occur in the vugs of rhodonite, they most likely precipitated from hydrothermal fluids rather than crystallize as a product of solid-state metamorphic growth.

The assemblage of sulfidic minerals present in manganese ore at the Prakovce–Zimná Voda occurrence the most probably originate from the hydrothermal fluids driven by tectono-metamorphic Alpine activity. Sulfides are mostly developed in cavities and veins suggesting their late formation. Presence of Co-rich phases indicates the adsorption of elements from the synsedimentary protolith (Rojkovič 2001). Furthermore, presence of hübnerite was also confirmed, suggesting interaction of manganese minerals with tungsten-rich fluids probably incorporated from the external source. The small quantity of sulfides in the manganese mineralization suggests their low mobility during metamorphic evolution. Some sulfides also exhibit a slightly higher Mn content (up to 0.09 *apfu*, Tab. 3), what is in good agreement with the other sulfides identified in manganese deposits in the Western Carpathian area. Elevated content of Mn in pyrite, sphalerite and cobaltite is quite common at the manganese deposits, however, Mn content in galena is rather unusual, as it was identified more preferably in experimental high temperature environments (Bethke and Barton 1971) in the range 600–800 ºC, what may indicate content of Mn in galena as an analytical artefact. The extremely low sulphide content in magnetite–manganese ore is due to the absence of suitable geological and petrological environments (such as lydites and graphitic phyllites), which provide the necessary source of sulphide-forming elements.

6. Conclusions

An association of manganese minerals was recently rediscovered and studied at the locality Zimná Voda near Prakovce village. Manganese ore is associated with the magnetite bodies and it is hosted in the metamorphosed acidic volcanoclastic material (mainly metarhyolites and their tuffs). Locality represents the first occurrence of metamorphosed manganese mineralization hosted in the metavolcano-sedimentary rocks of the Drnava Formation.

The genesis of manganese mineralization within magnetite bodies is linked to the bimodal early Paleozoic volcanic activity that formed strata-bound iron ores embedded in the volcano–sedimentary sequences of the Drnava Formation. Subsequent Variscan and Alpine metamorphic processes under the greenschist facies conditions mobilised elements and accumulated them in the suitable environments. Magnetite formation is considered to represent the earliest mineralization process, concurrent with the incorporation of manganese solutions into the system, forming rhodonite-ferrorhodonite series serving as matrix of manganese mineralization. The formation of manganese silicates is attributed to the elevated concentrations of silicon, aluminum, iron, and other elements in the quartz-rich acidic protolith, alongside with a gradual rise in P–T conditions, as well as the interaction of Mn-rich fluids with silicates.

The Zimná Voda occurrence is notable for its high magnetite content compared to the other currently known Western Carpathian deposits. Manganese ore primarily consists of a first-stage mineral assemblage that includes rhodonite–ferrorhodonite series, spessartine, rhodochrosite, kutnohorite, fluorapatite and quartz. The second stage of mineralization is characteristic by the development of cracks and cavities, which facilitated the formation of vein-type minerals such as rhodochrosite, kutnohorite, baryte, clino-suenoite, clino-ferro-suenoite, minerals of the epidote supergroup, quartz as well as sulfidic mineralization represented by pyrite, galena, sphalerite and cobaltite alongside with hübnerite. This stage is furthermore associated with the formation of garnets dominantly consisting of andradite, with locally preserved dissolved spessartine.

The Zimná Voda occurrence near Prakovce represents an exceptional locality as it marks the first finding of ferriallanite-(Ce), ferriallanite-(La), ferriakasakaite-(La) and ferriakasakaite-(Ce) among the manganese occurrences in the Western Carpathian contributing to the overall evolution of manganese mineralization. The formation of epidotes is the most probably linked to a low-grade Alpine metamorphic event indicating high mobility of rare earth elements (REE).

Acknowledgements. We are thankful to Editor František Laufek, as well as reviewers Radek Škoda and Pavel Uher for their helpful comments. We want to thank J. Sejkora who provided PXRD analyses of rhodonite. This study was financially supported by APVV-22-0041 and VEGA 2/0029/23 projects.

Electronic supplementary material. Supplementary data to this article can be found online at the Journal web site *(http://dx.doi.org/10.3190/jgeosci.400)*.

References

Anenburg M, Katzir Y, Rhede D, Jöns N, Bach W (2015) Rare earth element evolution and migration in plagiogranites: a record preserved in epidote and allanite of the Troodos ophiolite. Contrib Mineral Petr 169: 25

Armbruster T, Bonazzi P, Akasaka M, Bermanec V, Chopin C, Gieré R, Heuss-Assbichler S, Liebscher A, Menchetti S, Pan Y, Pasero M (2006) Recommended nomenclature of epidote-group minerals. Eur J Mineral 18: 551–567

Bajaník Š, Vozárová A, Hanzel V, Ivanička J, Mello J, Pristaš J, Reichwalder P, Snopko L, Vozár J (1983) Explanations to geological map of the Slovenské Rudohorie Mts.- Eastern part, 1 : 50 000. ŠGÚDŠ, Bratislava, pp 1–223 (in Slovak)

Bataleva YV, Kruk AN, Novoselov ID, Palyanov YN (2020) Formation of spessartine and CO_2 via rhodochrosite decarbonation along a hot subduction P–T path. Minerals 10: 703

Bethke PH, Barton PB (1971) Distribution of some minor elements between coexisting sulfide minerals. Econ Geol 66: 140–163

Biagioni C, Bonazzi P, Pasero M, Zaccarini F, Balestra C, Bracco R, Cirriotti ME (2019) Manganiakasakaite-(La) and ferriakasakaite-(Ce), two new epidote supergroup minerals from Piedmont, Italy. Minerals 9: 353

Bonazzi P, Holstam D, Bindi L, Nysten P, Capitani GC (2009) Multi-analytical approach to solve the puzzle of an allanite-subgroup mineral from Kesebol, Västra, Götaland, Sweden. Amer Miner 94: 121–134

Bosi F, Biagioni C, Pasero M. (2019) Nomenclature and classification of the spinel supergroup. Eur J Mineral 31: 183–192

Chukanov NV, Zubkova NV, Schäfer C, Varlamov DA, Ermolaeva VN, Polekhovsky YS, Jančev S, Pekov IV, Pushcharovsky DY (2018) New data on ferriakasakaite-(La) and related minerals extending the compositional field of the epidote supergroup. Eur J Mineral 30: 323–332

Dasgupta S (1997) P–T–*X* relationships during metamorphism of manganese-rich sediments: current status and future studies. In: Nicholson K, Hein JR, Buhn B, Dasgupta S (eds.) Manganese mineralization: geochemistry and mineralogy of terrestrial and marine deposits. GSL Spec Publ 119: 327–337

Faryad SW (1991) Metamorphosis of the sediments of the early Paleozoic of Gemericum Unit. Miner Slov 23: 315–324 (in Slovak)

Faryad SW (1994) Mineralogy of Mn-rich rocks from greenschist facies sequences of the Gemericum, West Carpathians, Slovakia. Neu Jb Mineral Mh 10: 464–480

Faryad W (1995) Determination of P-T conditions of metamorphism in the Spiš-Gemer Ore Mts. (Western Carpathians). Miner Slov 27: 9–19 (in Slovak)

Faryad SW, Klápová H, Nosál L (2010) Mechanism of formation of atoll garnet during high-pressure metamorphism. Mineral Mag 74: 111–126

Geiger CA, Rossman GR (2020) Micro- and nano-size hydrogarnet clusters and proton ordering in calcium silicate garnet: Part I. The quest to understand the nature of “water” in garnet continues. Amer Miner 105, 455–467

Girtler D, Tropper P, Hauzenberger C (2013) Androsite-(Ce) and ferriandrosite-(Ce) as indicator for low low-grade REE-mobility in the Veitsch Mn deposit (Styria). Mitt Österr Mineral Gesell 159: 56

Giuntoli F, Lanari P, Engi M (2018) Deeply subducted continental fragments – Part 1: Fracturing, dissolution–precipitation, and diffusion processes recorded by garnet textures of the central Sesia Zone (western Italian Alps). Solid Earth 9: 167–189

Grecula P (1982) Gemericum – a segment of the Paleotethys riftogenic pool. Miner Slov-monograph, Bratislava, pp 1–263 (in Slovak)

Grecula P, Dianiška I, Ďuďa R, Hurný J, Kobulský J, Kusák B, Malachovský P, Matula I, Rozložník O (1977) Geology, tectonics and metallogenesis of the eastern part of the Spišsko-gemerské rudohorie Mts., SGR – east, Cu + comprehensive evaluation. Geol priesk, Spišská Nová Ves, pp 1–390 (in Slovak)

Grecula P, Abonyi A, Abonyiová M, Antaš J, Bartalský B, Bartalský J, Dianiška I, Drzník E, Ďuďa R, Gargulák M, Gazdačko Ľ, Hudáček J, Kobulský J, Lörincz L, Macko J, Návesňák D, Németh Z, Novotný L, Radvanec M, Rojkovič I, Rozložník L, Rozložník O, Varček C, Zlocha J (1995) Mineral deposits of Slovak Ore Mountains. Miner Slov-monograph, pp 1–834 (in Slovak)

Grew ES, Locock AJ, Mills SJ, Galuskina IO, Galuskin EV, Hålenius U (2013) Nomenclature of the garnet supergroup. Amer Miner 98: 785–811

Hawthorne FC, Oberti R, Harlow GE, Maresch WV, Martin RF, Schumacher JC, Welch MD (2012) Nomenclature of the amphibole supergroup. Amer Miner 97: 2031–2048

Hein JR, Koschinsky A, Halbach P et al. (1997) Iron and Manganese Oxide Mineralization in the Pacific. In: Nicholson K, Hein JR, Buhn B et al. (eds.) Manganese Mineralization: Geochemistry and Mineralogy of Terrestrial and Marine Deposits. Geol Soc Spec Publ, 119: 123–138

Holtstam D, Andersson UB, Mansfeld J (2003) Ferriallanite-(Ce) from the Bastnäs deposit, Västmanland, Sweden. Canad Mineral 41: 1233–1240

Hsu LC (1968) Selected phase relationships in the system Al–Mn–Fe–Si–O–H: a model for garnet equilibria. J Petrol 9: 40–83

Ilavský J (1957) Geology of ore deposits in Spišsko-gemerské rudohorie Mts. Geol Práce, Zoš 46: 51–59 (in Slovak)

Kantor J (1953a) Manganese deposit on Hekerová (Bystrý potok) west of Smolník. Manuscript, ŠGÚDŠ, Bratislava, pp 1–30 (in Slovak)

Kantor J (1953b) Manganese deposit near Čučma. Manuscript, ŠGÚDŠ, Bratislava, pp 1–32 (in Slovak)

Kantor J (1954) On the genesis of manganese ores in the Spišsko-gemerské rudohorie Mts. Geol Práce, Zpr 1: 70–71 (in Slovak)

Kartashov PM, Ferraris G, Ivaldi G, Sokolova E, McCammon CA (2002): Ferriallanite-(Ce) $\mathrm{CaCeFe^{3+}AlFe^{2+}(SiO_4)(Si_2O_7)O(OH)}$, a new member of the edpidote group: description, X-ray and Mössbauer study. Canad Mineral 40:1641–1648

Kasatkin AV, Zubkova NV, Pekov IV, Chukanov NV, Škoda R, Polekhovsky YS, Agakhanov AA, Belakovskiy DI, Kuznetsov AM, Britvin SN, Pushcharovsky DY (2020) The mineralogy of the historical Mochalin Log REE deposit, South Urals, Russia. Part I. New gatelite-group minerals ferriperbøeite-(La), $\mathrm{(CaLa_3)Fe^{3+}Al_2Fe^{2+})}$ $\mathrm{[Si_2O_7][SiO_4]_3O(OH)_2}$ and perbøeite-(LA), $\mathrm{(CaLa_3)}$ $\mathrm{(Al_3Fe^{2+})[Si_2O_7][SiO_4]_3O(OH)_2}$. Mineral Mag 84: 593–607

Kolitsch U, Mills SJ, Miyawaki R, Blass G (2012) Ferriallanite-(La), a new member of the epidote supergroup from the Eifel, Germany. Eur J Mineral 24: 741–747

Konrad-Schmolke M, O´Brien PJ, Heidelbach F (2007) Compositional re-equilibration of garnet: the importance of sub-grain boundaries. Eur J Mineral 19: 431–438

Kuleshov V, Maynard JB (2017) Isotope Geochemistry: The origin and formation of manganese rocks and ores. Elsevier Science, pp 1–427

Leonhard G (1843) Concise dictionary of topographic mineralogy. Heidelberg Academy. Publishing act by J. C. B. Mohr, pp 1–593 (in German)

Mazzoli C, Vozárová A (1989) Further data concerning the pressure character of the Hercynian metamorphism in the West Carpathians (Czechoslovakia). Rc Soc Ital Mineral Petrol 43: 635–342

Melcher F (1995) Genesis of chemical sediments in Birimian greenstone belts: evidence from gondites and related manganese-bearing rocks from Northern Ghana. Mineral Mag 59: 229–251

Myšľan P, Ružička P (2022) Micas and chlorites as indicators of metamorphic conditions of carbonate rocks of the Gelnica Group in the Souther Gemericum (Slovak Republic). Bull Mineral Petrol 30: 108–123 (in Slovak)

Myšľan P, Števko M, Mikuš T (2023) Mineralogy and genetic aspects of the metamorphosed manganese mineralization at the Július ore occurrence near Betliar (Gemeric Unit, Western Carpathians, Slovakia). J Geosci 68: 313–332

Myšľan P, Števko M, Mikuš T, Vrtiška L (2024) Mineralogy and genetic considerations of the metamorphosed As-rich manganese ore mineralization at the Diely occurrence near Poráč (Northern Gemeric Unit, Western Carpathians, Slovakia). Mineral Mag (*in press*)

Nagashima M, Imaoka T, Nakashima K (2011) Crystal chemistry of Ti-rich ferriallanite-(Ce) from Cape Ashizuri, Shikoku Island, Japan. Amer Miner 96: 1870–1877

Nagashima M, Nishio-Hamane D, Tomita N, Minakawa T, Inaba S (2015) Ferriakasakaite-(La) and ferriandrosite-(La): new epidote-supergroup minerals from Ise, Mie Prefecture, Japan. Mineral Mag 79: 735–753

Nyame FK (2001) Petrological significance of manganese carbonate inclusions in spessartine garnet and relation to the stability of spessartine in metamorphosed manganese-rich rocks. Contrib Mineral Petr 141: 733–746

Oberti R, Boiocchi M, Hawthorne FC, Ciriotti ME, Revheim O, Bracco R (2018) Clino-suenoite, a newly approved magnesium–iron–manganese amphibole from Valmalenco, Sondrio, Italy. Mineral Mag 82: 189–198

Peterec D, Ďuďa R (2003) Rare minerals of Mn deposit near Čučma. Natur Carpath 44: 229–236 (in Slovak)

Putiš M, Sergeev S, Ondrejka M, Larionov A, Siman P, Spišiak J, Uher P, Paderin I (2008) Cambrian–Ordovician metaigneous rocks associated with Cadomian fragments in the West-Carpathian basement dated by SHRIMP on zircons: A record the Gondwana active margin setting. Geol Carpath 59: 3–18

Radvanec M, Gonda S (2020) Successive formation of Fe and Mn skarns in the Čučma locality (Gemeric unit, W. Carpathians): from metasomatic stage through the amphibolite facies overprint with Ti-rich tephroite to retrograde stilpnomelane–chlorite zone. Miner Slov 52: 103–132

Rojkovič I (1999) Manganese mineralization in the Wester Carpathians, Slovakia. Geol Carpath, Special Issue 50: 191–192

Rojkovič I (2001) Early Paleozoic Manganese ores in the Gemericum Superunit, Western Carpathians, Slovakia. Geolines 13: 34–41

Roy S (1981) Manganese deposits. Academic Press, London; New York, pp 1–458

Roy S (1992) Environments and Processes of Manganese Deposition. Econ Geol 87: 1218–1236

Ružička P, Bačík P, Myšľan P, Kurylo S (2020) Grossular and diopside in crystalline limestone from the locality Čučma–Čierna baňa (Slovak Republic). Bull Mineral Petrol 28: 94–104 (in Slovak)

Sassi R, Vozárová A (1987) The pressure character of the Hercynian metamorphism in the Gemericum (West Carpathians, Czechoslovakia). Rc Soc Ital Mineral Petrol 42: 73–81

Shchipalkina NV, Chukanov NV, Pekov IV, Aksenov SM, McCammon C, Belakovskiy D, Britvin SN, Koshlykova NN, Schäfer C, Scholz R, Rastsvetaeva RK (2017) Ferrorhodonite, $CaMn_3Fe[Si_5O_{15}]$, a new mineral species from Broken Hill, New South Wales, Australia. Phys Chem Miner 44: 323–334

Shchipalkina NV, Pekov IV, Chukanov NV, Biagioni C, Pasero M (2019) Crystal chemistry and nomenclature of rhodonite-group minerals. Mineral Mag 83: 829–835

Snopko L, Vozárová A (1981) Lithological and petrographic research of the Drnava Formation of the Gelnica Group. Západné Karpaty, Séria Mineralógia, petrografia, geochémia, metalogenéza 9: 111–144 (in Slovak)

Snopková P, Snopko L (1979) Biostratigraphy of the Gelnica series in the Spišsko-gemerské rudohorie Mts. based on palynological results (Western Carpathians, Paleozoic). Západné Karpaty, Sér geol 5: 57–102 (in Slovak)

Sobek K, Losos Z, Škoda Z, Holá M, Nasdala L (2023) Crystal chemistry of ferriallanite-(Ce) from Nya Bastnäs, Sweden: Chemical and spectroscopic study. Mineral Petrol 117: 345–357

Spišiak J, Hovorka D (2000) Piemontite and spessartine in lower paleozoic metasediments of the inner Western Carpathians. Acta Mineral Petrogr 41: 102

Spišiak J, Hovorka D, Rybka R, Turan J (1989) Spessartine and piemontite in Lower Paleozoic metasediments of the Inner West Carpathians. Čas Mineral Geol 34: 17–30 (in Slovak)

Števko M, Plecháček J, Venclík V, Malíková R (2015) Hausmannite a manganosite from the Čučma–Čierna baňa manganese deposit (Slovak Republic). Bull Mineral Petrol 23: 39–42

Števko M, Myšľan P, Biagioni C, Mauro D, Mikuš T (2023) Ferriandrosite-(Ce), a new member of the epidote supergroup from Betliar, Slovakia. Mineral Mag 87: 887–895

Theye T, Schreyer W, Fransolet A-M (1996) Low-temperature, low-pressure metamorphism of Mn-rich rocks in the Lienne Syncline, Venn-Stavelot Massif (Belgian Ardennes) and the role of carpholite. J Petrol 37: 767–783

Uher P, Broska I (1996) Post-orogenic Permian granitic rocks in the Western Carpathian–Pannonian area: Geochemistry, mineralogy and evolution. Geol Carpath 47: 311–321

Uher P, Ondrejka M, Bačík P, Broska I, Konečný P (2015) Britholite, monazite, REE carbonates, and calcite: Products of hydrothermal alteration of allanite and apatite in A-type granite from Stupné, Western Carpathians, Slovakia. Lithos 236-237: 212–225

Varlamov DA, Ermolaeva VN, Chukanov NV, Jančev S, Vigasina MF, Plechov PYu (2019) New data on epidote-supergroup minerals: Unusual chemical composition, typochemistry, and Raman spectroscopy. Geol Ore Deposits 61: 827–842

Vlach SRF (2022) On the morphology and geochemistry of hydrothermal crypto-and microcrystalline zircon aggregates in a peralkaline granite. Minerals 12: 628

Vozárová A, Rodionov N, Šarinová K, Presnyakov S (2017) New zircon ages on the Cambrian–Ordovician volcanism of the Southern Gemericum basement (Western Carparthians, Slovakia): SHRIMP dating, geochemistry and provenance. Int J Earth Sci 106: 2147–2170

Warr LN (2021) IMA-CNMNC approved mineral symbols. Mineral Mag 85: 291–320

Whitney DL, Mechum TA, Dilek Y, Kuehner SM (1996) Modification of garnet by fluid infiltration during regional metamorphism in garnet through sillimanite-zone rocks, Dutchess County, New York. Amer Miner 81: 696–705

Zipser CA (1817) An attempt at a topographical-mineralogical handbook of Hungary. Carl Friedrich Wigand, Oedenburg, pp 1–440 (in German)